ELSEVIER

Journal of Fluids and Structures 24 (2008) 932–953

JOURNAL OF FLUIDS AND STRUCTURES

www.elsevier.com/locate/jfs

Dynamics of trains and train-like articulated systems travelling in confined fluid—Part 1: Modelling and basic dynamics

Y. Sakuma*, M.P. Païdoussis, S.J. Price

Department of Mechanical Engineering, McGill University, 817 Sherbrooke Street West, Montreal, Québec, Canada H3A 2K6

Received 24 October 2006; accepted 5 January 2008
Available online 9 May 2008

Abstract

The dynamics and stability of a train of flexibly interconnected rigid cylinders travelling in a confined cylindrical "tunnel" subjected to fluid dynamic forces is studied theoretically. Each cylinder, which is coupled to other cylinders and supported by springs and dampers, has degrees of freedom in the lateral translational and rotational directions. The kinetic, dissipation, and potential energies of the system and the generalized forces associated with the fluid dynamic forces acting on the system, such as inviscid fluid dynamic forces, viscous frictional forces, and form drag, are obtained first. Then the equations of motion are derived in a Lagrangian framework. The principal aim of this study is to investigate the effect of the aerodynamic forces on the dynamics of a high-speed train running in a tunnel, or more generally of a train-like system travelling in a coaxial cylindrical tube. The results of this study show that the system loses stability by flutter and that viscous frictional drag has a considerable effect on stability of the system. In addition, the mechanism of instability of the system is clarified with the aid of a study of the modal shapes and energy considerations.
© 2008 Elsevier Ltd. All rights reserved.

Keywords: Trains; Articulated systems; Aerodynamic forces; Spatially periodic structures; Train in tunnel

1. Introduction

The instabilities of cylindrical structures in axial flow were studied, first theoretically and then experimentally, in the 1960s by Païdoussis (1966a, b) for systems in unconfined flow. Similar work was conducted for towed cylinders, displaying a more intricate dynamical behaviour (Hawthorne, 1961; Païdoussis, 1968). This theory was extended, corrected, and generalized later (Païdoussis, 1973).

Interest in the dynamical behaviour of articulated cylindrical systems in external axial flow is more recent than that of the continuous (distributed-parameter) system. Work was done in conjunction with the dynamics of (i) fuel "strings" or "stringers" of certain types of nuclear reactors (Païdoussis, 1976), and (ii) underwater systems towed by a submarine (Hamy, 1971; Païdoussis, 1970, 1986).

Annular flow over structures may be seen as an intermediate situation between external and internal axial flow in or around structures. An analytical model for very narrow annular configurations was developed by Païdoussis et al.

*Corresponding author. Present address: Railway Technical Research Institute, Aerodynamics Laboratory, 2-8-38 Hikari-cho, Kokubunji-shi, Tokyo, 185-8540, Japan.
E-mail address: sakuma@rtri.or.jp (Y. Sakuma).

0889-9746/$ - see front matter © 2008 Elsevier Ltd. All rights reserved.
doi:10.1016/j.jfluidstructs.2008.01.002

(1990), adapting for a flexible cylinder Mateescu and Païdoussis's (1985, 1987) work on the stability of rigid centrebodies. A similar analytical model was also developed by Fujita and Shintani (2001), in the spirit of the Inada and Hayama (1990a, b), Porcher and de Langre (1997), and Fujita et al. (2000) models for rigid bodies in annular flow; the main findings in the former have thereby been reconfirmed in the latter studies.

Some attempts have been made in the past to analyse the dynamics of train-like systems in fluids. Incompressible inviscid slender-body theory was used to determine the flow about a slender body of revolution travelling in a tube (Goodman, 1967; Goodman and Lehman, 1968; Wang, 1969). The dynamical stability of underwater transportation systems in unconfined space was studied by Païdoussis (1986). Aeroelastic stability of an Euler–Bernoulli beam travelling in a tunnel lined with Helmholtz resonators was studied by Sugimoto (1996). The aerodynamically excited vibration of coupled rigid bodies in a tunnel due to leakage flow was recently studied theoretically and experimentally by Tanaka et al. (1999, 2001). The interested reader is referred to Païdoussis (1998, 2003) for additional references.

The configurations in the above studies are considered to be too simple to properly model the structure of actual above-ground trains. Hence, the present work employs a more realistic model of the train structure, yet simple enough for examining with ease the fluid–train interactions in a tunnel. That is, this work develops a general approach for the study of the dynamics of trains and train-like systems of flexibly interconnected rigid cylinders with elastic supports subjected to fluid dynamic forces and moving in a tunnel. Moreover, the mechanism of instability of the system is clarified with the aid of the computed modal shapes and energy considerations, i.e. by examining the work done by the fluid on the system.

2. Theoretical model of the dynamics

2.1. Description of the system and assumptions

In order to achieve a description of the overall motion of a train passing through a tunnel, a large number of simplifying idealizations have to be introduced. Simulation of translational and rotational motions of train dynamics commonly includes seventeen and more degrees of freedom for each car and interaction between wheels and rails (Miyamoto, 1994). Since the main concern of the present study is to examine the effect of the aerodynamic forces on trains and train-like articulated systems, the simplest approach has been adopted to model the structure of bogies. A vehicle with two bogies is simplified to a cylindrical body supported only on two sets of translational springs and dampers, i.e. the bogies are modelled by springs and dampers. These cylindrical cars are coupled by springs and dampers and they can perform translational and rotational oscillatory motions in a cylindrical duct. It is assumed that there is no slip between the wheels and the rails in the lateral direction. With this assumption, this approximation of the rails' reaction against the lateral wheel motion by a spring-dashpot element is fully justified. It should be mentioned, however, that only the onset of the train instability can be analysed under this assumption. Moreover, the system is modelled with the aid of certain additional assumptions, which are presented in the following.

The system under consideration is shown in Fig. 1. It consists of N rigid cylindrical cars that can only perform lateral translational $y^*(t)$ and yawing $\alpha(t)$ oscillatory motions of small amplitude in the cylindrical duct. Each car is attached to the duct (effectively to the rails or the "ground") via two sets of translational springs and dampers (k_f, k_b, c_f, and c_b; "f" for front, "b" for back). Rotational and translational springs and dampers are also considered interconnecting the cars (k_η, k_α, c_η, and c_α). The leading and trailing cars comprise streamlined ends. U is the flow velocity in the space between the sides of the train and the tunnel in the train coordinate system. It is assumed that the annular flow is not disturbed by the existence of the springs and dampers. The following assumptions are also made: (a) the fluid is incompressible and of uniform density; (b) no local separation of the flow takes place; and (c) boundary layer development on the tunnel walls is ignored.

The forces associated with the structure itself are taken into account in the kinetic, dissipation, and potential energies of the system. Concerning the fluid forces, they could in principle be determined by an appropriate solution of the Navier–Stokes equations. This will not be attempted here; instead, the fluid forces are determined essentially by superposition: inviscid and viscous forces are determined separately, based on Païdoussis's work. This has been shown to be quite acceptable (Païdoussis, 1973, 1986), even for more complex systems (Païdoussis, 1979). The hydrodynamic forces are incorporated partly in the kinetic energy and partly as generalized forces.

To obtain the equations of motion by application of the Lagrange equations, we now proceed to formulate the kinetic, dissipation, and potential energies of the system and the generalized forces.

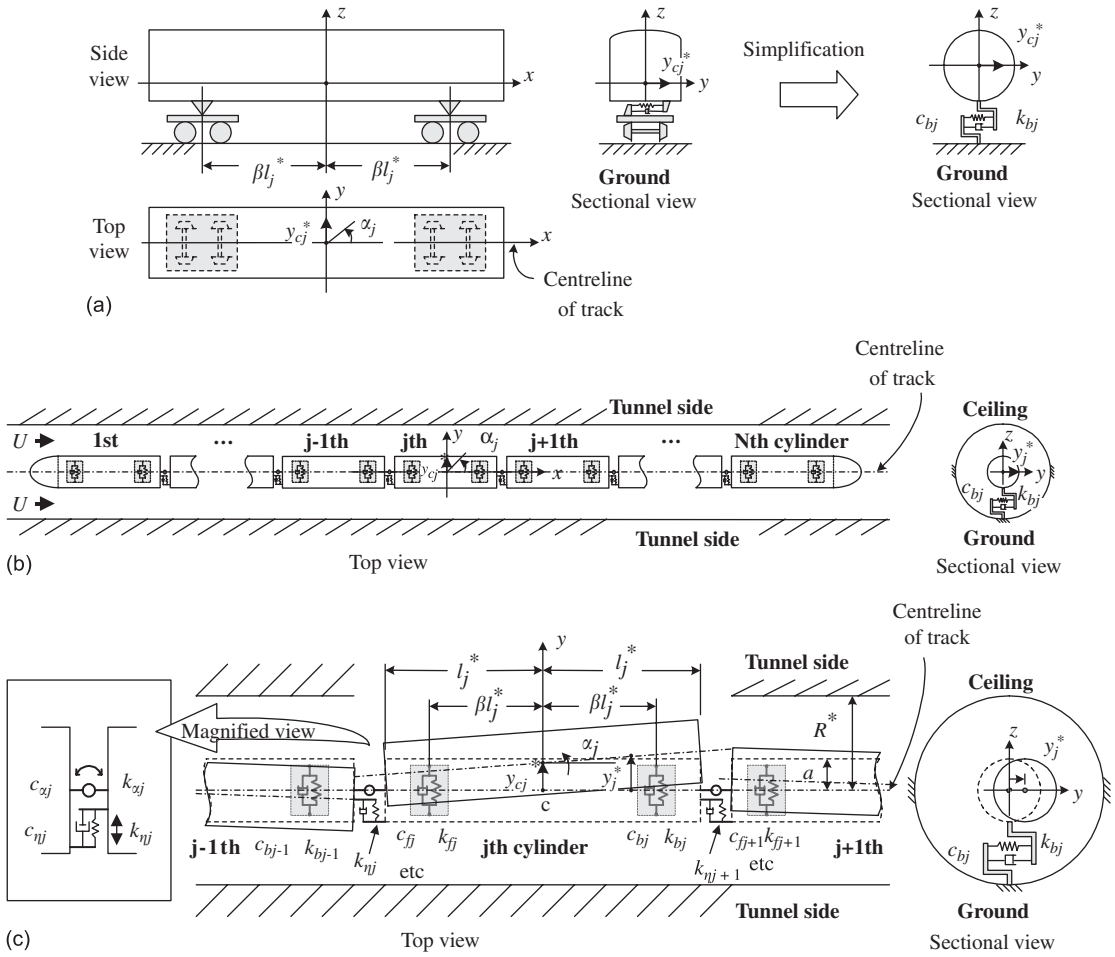

Fig. 1. Geometry of (a) a vehicle and a simplified cylindrical car, (b) N interconnected rigid cylindrical cars, and (c) the jth oscillating cylindrical car in the cylindrical duct. The variables with an asterisk are dimensional quantities.

2.2. Kinetic, dissipation, and potential energies of the structure

The kinetic energy of the jth car, T_{sj}, is

$$T_{sj} = \tfrac{1}{2} m_j \dot{y}^*_{cj}(t)^2 + \tfrac{1}{2} J_{cj} \dot{\alpha}_j(t)^2, \tag{1}$$

where m_j is the mass of the jth car and J_{cj} is its mass-moment of inertia about the centre of mass.

The dissipation energy of the jth car, D_{sj}, is

$$\begin{aligned} D_{sj} = {} & \tfrac{1}{2} c_{fj} (\dot{y}^*_{cj} - \beta l^*_j \dot{\alpha}_j)^2 + \tfrac{1}{2} c_{bj} (\dot{y}^*_{cj} + \beta l^*_j \dot{\alpha}_j)^2 + \tfrac{1}{2} c_{\alpha j} (\dot{\alpha}_j - \dot{\alpha}_{j-1})^2 + \tfrac{1}{2} c_{\eta j} \{(\dot{y}^*_{cj} - l^*_j \dot{\alpha}_j) - (\dot{y}^*_{cj-1} + l^*_{j-1} \dot{\alpha}_{j-1})\}^2 \\ & + \tfrac{1}{2} c_{\alpha j+1} (\dot{\alpha}_{j+1} - \dot{\alpha}_j)^2 + \tfrac{1}{2} c_{\eta j+1} \{(\dot{y}^*_{cj+1} - l^*_{j+1} \dot{\alpha}_{j+1}) - (\dot{y}^*_{cj} + l^*_j \dot{\alpha}_j)\}^2, \end{aligned} \tag{2}$$

where β is the displacement coefficient for the supporting spring from the centre of the car as shown in Fig. 1(a) and l^*_j is the half length of the jth car.

Finally, the potential energy of the jth car, V_{sj}, is

$$\begin{aligned} V_{sj} = {} & \tfrac{1}{2} k_{fj} (y^*_{cj} - \beta l^*_j \alpha_j)^2 + \tfrac{1}{2} k_{bj} (y^*_{cj} + \beta l^*_j \alpha_j)^2 + \tfrac{1}{2} k_{\alpha j} (\alpha_j - \alpha_{j-1})^2 + \tfrac{1}{2} k_{\eta j} \{(y^*_{cj} - l^*_j \alpha_j) - (y^*_{cj-1} + l^*_{j-1} \alpha_{j-1})\}^2 \\ & + \tfrac{1}{2} k_{\alpha j+1} (\alpha_{j+1} - \alpha_j)^2 + \tfrac{1}{2} k_{\eta j+1} \{(y^*_{cj+1} - l^*_{j+1} \alpha_{j+1}) - (y^*_{cj} + l^*_j \alpha_j)\}^2. \end{aligned} \tag{3}$$

2.3. Kinetic energy of the fluid

The conservative inviscid part of the fluid dynamic forces can be included in the total kinetic energy of the system. Lighthill's (1960) work, which is essentially an application of slender-body theory, is adopted. By this theory, the normal flow velocity at any point ξ of the jth car is calculated.

We describe the coupled car system subjected to external axial flow as "straight" when it is stationary along the x-axis, such that no resultant normal force acts on its cross-section. Then, as shown in Fig. 2, we suppose that the system has a displacement $y^*(x,t)$ from the straight position in the y-direction. We isolate an element of a car (say, the jth one) as in Fig. 2, and then, by slender-body theory, the transverse flow velocity may be regarded as being composed of (a) a component associated with the steady flow around the straight body, in which case the flow velocity is $U\cos\alpha_j \simeq U$ and (b) the reversed flow velocity due to the displacement $y_j^*(x,t)$. Hence, the relative fluid-body velocity in the direction normal to the element is $v_{fj}(x,t) = (\partial y_j^*/\partial t)\cos\alpha_j + U\sin\alpha_j$. Note that $(\partial y_j^*/\partial x) = \alpha_j$. For small α_j, $\cos\alpha_j \simeq 1$, $\sin\alpha_j \simeq \tan\alpha_j = \partial y_j^*/\partial x^*$; therefore,

$$v_{fj}(x,t) = \frac{\partial y^*}{\partial t} + U\frac{\partial y^*}{\partial x^*}. \tag{4}$$

The lateral displacement of the element of the jth car, y_j^*, is given by

$$y_j^*(t) = y_{cj}^*(t) + \xi^*\alpha_j(t), \tag{5}$$

where ξ^* is the local coordinate on the jth car, which is related to the x coordinate by

$$x^* = 2\sum_{k=1}^{j-1} l_k^* + l_j^* + \xi^* = L_j^* + \xi^*, \tag{6}$$

where $L_j^* = 2\sum_{k=1}^{j-1} l_k^* + l_j^*$ is the middle point of the jth car. Then, the lateral velocity of the fluid on the inclined jth car moving laterally is given by

$$v_{fj}(\xi^*) = \dot{y}_j^*(t) = \dot{y}_{cj}^*(t) + \xi^*\dot{\alpha}_j(t) + U\alpha_j(t). \tag{7}$$

The kinetic energy of the lateral fluid flow around the jth car is

$$T_{fj} = \int_{-l_j^*}^{l_j^*} \tfrac{1}{2}Mv_{fj}^2(\xi^*)\,\mathrm{d}\xi^*, \tag{8}$$

where $M = \chi\rho A$ is the virtual mass of the fluid, ρ is the fluid density, A is the cross-sectional area of the car, and $\chi = (R^{*2} + a^2)/(R^{*2} - a^2)$, where a is the radius of the cylindrical car and R^* the tunnel radius, is related to confinement by the tunnel. Substituting Eq. (7) into Eq. (8), one obtains

$$T_{fj} = \chi\rho A l_j^*\{\tfrac{1}{3}l_j^{*2}\dot{\alpha}_j(t)^2 + (\dot{y}_{cj}^*(t) + U\alpha_j(t))^2\}. \tag{9}$$

2.4. The generalized forces on a middle (jth) car

Next, the generalized forces will be obtained. Forces other than the conservative inviscid fluid dynamic forces acting on the system are shown in Fig. 3: viscous forces, pressure gradient forces, nonconservative inviscid forces, and form drag. Recall that the conservative component of the inviscid forces has been expressed as a kinetic energy equation (9).

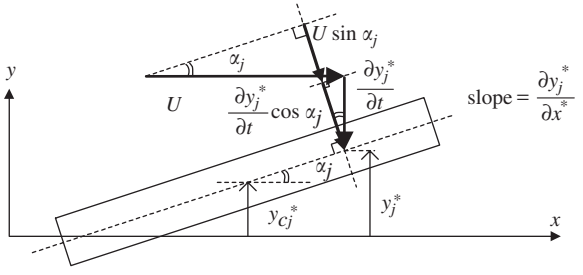

Fig. 2. Calculation of the relative fluid-body velocity in the normal direction of the jth cylindrical car.

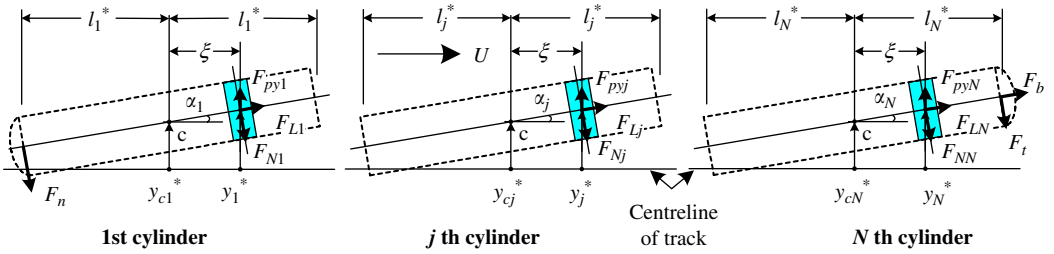

Fig. 3. Forces acting on cylindrical cars and on elements $d\xi$ of the 1st, jth, and Nth cylindrical cars.

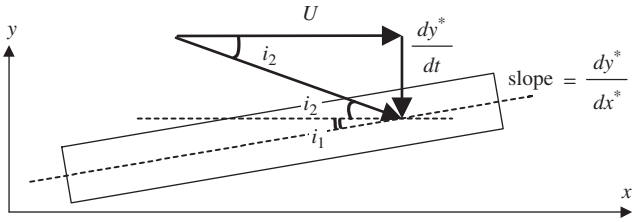

Fig. 4. Calculation of the angle of incidence i of the cylindrical car, $i = i_1 + i_2$.

Apart from the leading ($j = 1$) and trailing ($j = N$) cars, two aerodynamic forces (other than the inviscid ones) act on the middle cars ($j = 2, \ldots, N$): viscous and pressure gradient forces, as shown in Fig. 3.

The viscous forces per unit length of the jth car in the normal and longitudinal directions F_{Nj} and F_{Lj} are as given by Taylor (1952):

$$F_{Nj} = \tfrac{1}{2}\rho D^* U^2 (C_N \sin i + C_{Dp} \sin^2 i), \quad F_{Lj} = \tfrac{1}{2}\rho D^* U^2 C_T \cos i, \tag{10}$$

where $i = \tan^{-1}(\partial y^*/\partial x^*) + \tan^{-1}\{(\partial y^*/\partial t)/U\}$ is the angle of inclination of the car to the flow, as shown in Fig. 4; D^* is the car diameter, C_N and C_T are the frictional drag coefficients in the normal and tangential directions, respectively, and C_{Dp} is the form drag coefficient. For small $\partial y^*/\partial x^*$ and $(\partial y^*/\partial t)/U$, Eq. (10) may be written as

$$F_{Nj} = \frac{1}{2}\rho D^* U C_N \left(\frac{\partial y_j^*}{\partial t} + U\frac{\partial y_j^*}{\partial x^*}\right) + \frac{1}{2}\rho D^* C_D \left(\frac{\partial y_j^*}{\partial t}\right), \quad F_{Lj} = \frac{1}{2}\rho D^* U^2 C_T, \tag{11}$$

where the second term in F_N represents a linearization of the quadratic viscous force at zero flow velocity, $\frac{1}{2}\rho D^* C_{Dp} |\partial y_j^*/\partial t| (\partial y_j^*/\partial t)$, in which the drag coefficient represents $C_D = C_{Dp} |\partial y_j^*/\partial t|$.

The pressure gradient forces in the x and y directions acting on the jth car equipped with hoods are given by

$$F_{px,j} = -2l_j^* A(1-\varepsilon)\frac{dp}{dx}, \quad F_{py,j} = -2l_j^* A(1-\varepsilon)\frac{dp}{dx}\alpha_j, \tag{12}$$

where ε is the ratio of cross-sectional area of the hood to that of the car. The pressure gradient distribution may be written as

$$A\frac{dp}{dx} = -\frac{1}{2}\rho D^* U^2 C_T \left(\frac{D^*}{D_h^*}\right) = -\frac{\rho a U^2 C_T}{r_h}, \tag{13}$$

where $D_h^* = 2(R^* - a)$ is the hydraulic diameter and $r_h = (R^* - a)/a$ is the ratio of the gap to the car radius.

The virtual work associated with the virtual displacement δW_j on the jth car is given by

$$\delta W_j = \int_{-l_j^*}^{l_j^*} (-F_{Nj} + F_{Lj}\alpha_j(t))\delta(y_{cj}^*(t) + \xi^*\alpha_j(t))\, d\xi^* + \delta W_{pj}. \tag{14}$$

Substituting Eqs. (11)–(13) into Eq. (14), we obtain the generalized forces Q_{ycj} and $Q_{\alpha j}$ on the jth car, respectively, associated with translational and rotational motions:

$$Q_{ycj} = \left.\frac{\delta W_j}{\delta y_{cj}^*}\right|_{\delta\alpha_j = 0} = -\rho D^*(UC_N + C_D) l_j^* \dot{y}_{cj}^*(t) + 2\left\{(\varepsilon - 1)A\frac{dp}{dx^*} + \frac{1}{2}\rho D^* U^2 + (C_T - C_N)\right\} + l_j^* \alpha_j(t), \tag{15}$$

$$Q_{\alpha j} = \left.\frac{\delta W_j}{\delta \alpha_j}\right|_{\delta y^*_{cj}=0} = -\frac{1}{3}\rho D^*(UC_N + C_D) l_j^{*3}\dot{\alpha}_j(t). \tag{16}$$

2.5. Additional generalized forces on the leading (1st) and trailing (Nth) cars

For the first and Nth cars, in addition to the forces already formulated for any "middle car," nonconservative inviscid forces, F_n and F_t ("n" for nose, "t" for tail), and a form drag F_b act on the leading ($j = 1$) and trailing ($j = N$) cars, respectively, as shown in Fig. 3.

If both ends of the system were supported, the summation of expression (9) over all the cars from $j = 1$ to N would represent the whole of the inviscid component of the fluid dynamic forces. However, the present system of the train is nonconservative, and hence there will generally be work done at the free end of the system by the nonconservative lateral inviscid forces, F_n and F_t (Hawthorne, 1961; Païdoussis, 1966a).

These nonconservative inviscid forces acting on the nose and tail of the system, F_n and F_t, may be written as

$$F_n = -(1-f_n)\chi\rho AU\left(\frac{\partial y_1^*}{\partial t} + U\frac{\partial y_1^*}{\partial x^*}\right), \quad F_t = -(1-f_t)\chi\rho AU\left(\frac{\partial y_N^*}{\partial t} + U\frac{\partial y_N^*}{\partial x^*}\right), \tag{17}$$

where f_n and f_t are parameters that are equal to or less than unity, which take into account loss in lateral momentum flux due to the shape of the free end; for an ideally streamlined end, $f_n \to 1$ or $f_t \to 1$ (Païdoussis, 1966a, 1973).

The form drag of the trailing car, F_b, associated with separation of the flow is given by

$$F_b = \tfrac{1}{2}\rho D^{*2} U^2 C_b, \tag{18}$$

where C_b is the base drag coefficient.

The virtual work associated with the first car δW_1 will therefore have the additional term

$$\delta W'_1 = F_n \delta y^*_{c1}(t) - F_n l_1^* \delta\alpha_1(t). \tag{19}$$

Hence, the additional generalized forces Q'_{yc1} and $Q'_{\alpha 1}$ on the first car are

$$Q'_{yc1} = \left.\frac{\delta W'_1}{\delta y^*_{c1}}\right|_{\delta\alpha_1=0} = F_n = -\chi(1-f_n)\rho AU\{\dot{y}^*_{c1}(t) - l_1^*\dot{\alpha}_1(t) + U\alpha_1(t)\}, \tag{20}$$

$$Q'_{\alpha 1} = \left.\frac{\delta W'_1}{\delta \alpha_1}\right|_{\delta y^*_{c1}=0} = -F_n l_1^* = \chi(1-f_n)\rho AU l_1^*\{\dot{y}^*_{c1}(t) - l_1^*\dot{\alpha}_1(t) + U\alpha_1(t)\}. \tag{21}$$

The virtual work associated with the last car δW_N will have the additional term

$$\delta W'_N = \{F_t + F_b\alpha_N(t)\}\delta(y^*_{cN}(t) + l_N^*\alpha_N(t)). \tag{22}$$

Therefore, the additional generalized forces Q'_{ycN} and $Q'_{\alpha N}$ on the last car are

$$\begin{aligned} Q'_{ycN} &= \left.\frac{\delta W'_N}{\delta y^*_{cN}}\right|_{\delta\alpha_N=0} = F_t + F_b\alpha_N(t) \\ &= -\chi(1-f_t)\rho AU\{\dot{y}^*_{cN}(t) + l_N^*\dot{\alpha}_N(t) + U\alpha_N(t)\} + \tfrac{1}{2}\rho D^2 U^2 C_b\alpha_N(t), \end{aligned} \tag{23}$$

$$\begin{aligned} Q'_{\alpha N} &= \left.\frac{\delta W'_N}{\delta \alpha_N}\right|_{\delta y^*_{cN}=0} = \{F_t + F_b\alpha_N(t)\} l_N^* \\ &= \left[-\chi(1-f_t)\rho AU\{\dot{y}^*_{cN}(t) + l_N^*\dot{\alpha}_N(t) + U\alpha_N(t)\} + \tfrac{1}{2}\rho D^2 U^2 C_b\alpha_N(t)\right] l_N^*. \end{aligned} \tag{24}$$

2.6. The equations of motion

The total kinetic energy of the system, T, is given by $T = T_s + T_f$, where $T_s = \sum_{j=1}^N T_{sj}$ and $T_f = \sum_{j=1}^N T_{fj}$ are given by Eqs. (1) and (9), respectively. Similarly, $D = \sum_{j=1}^N D_{sj}$ and $V = \sum_{j=1}^N V_{sj}$. Eqs. (1)–(3), (9), and (15)–(24), while taking the summation over j into the account, are substituted into the Lagrange equations

$$\frac{\mathrm{d}}{\mathrm{d}t}\left(\frac{\partial T}{\partial \dot{q}_i}\right) - \frac{\partial T}{\partial q_i} + \frac{\partial D}{\partial \dot{q}_i} + \frac{\partial V}{\partial q_i} = Q_i, \quad q_1 = y^*_{cj}, \quad q_2 = \alpha_j, \quad j = 1, 2, \ldots, N,$$

which yields the equations of motion. Introducing the dimensionless quantities

$$x = x^*/a, \quad y = y^*/a, \quad l = l^*/a, \quad D = D^*/a = 2, \quad \tau = t\sqrt{\frac{k_0}{m_0 a}}, \quad u = U\sqrt{\frac{m_0}{k_0 a}},$$

$$\omega = \Omega\sqrt{\frac{m_0 a}{k_0}}, \quad \mu = \frac{M_0}{m_0}, \quad \overline{k}_{\eta j} = \frac{k_{\eta j}}{k_0}, \quad \overline{k}_{\alpha j} = \frac{k_{\alpha j}}{a^2 k_0},$$

$$\zeta_{\eta j} = \frac{c_{\eta j}}{\sqrt{k_0 m_0 a}}, \quad \zeta_{\alpha j} = \frac{c_{\alpha j}}{a^2\sqrt{k_0 m_0 a}}, \quad c = C_D\sqrt{\frac{m_0}{k_0 a}},$$

into the equations of motion, where k_0 is the reference coefficient of translational spring between the cylinders and the duct, m_0 the mass of cylinder per unit length, and M_0 the virtual mass of the fluid per unit length of the cylinder, we obtain the dimensionless equations of motion for constant frictional viscous forces along the train:

$$\begin{aligned}
&2(1+\chi\mu)l_j\frac{\mathrm{d}^2 y_{cj}(\tau)}{\mathrm{d}\tau^2} + \delta_{j1}\chi\mu(1-f_n)u\frac{\mathrm{d}y_{c1}(\tau)}{\mathrm{d}\tau} - \zeta_{\eta j}\frac{\mathrm{d}y_{cj-1}(\tau)}{\mathrm{d}\tau}\\
&\quad + \left\{\zeta_{fj} + \zeta_{bj} + \zeta_{\eta j} + \zeta_{\eta j+1} + \frac{2\mu l_j}{\pi}(uC_N + c)\right\}\frac{\mathrm{d}y_{cj}(\tau)}{\mathrm{d}\tau} - \zeta_{\eta j+1}\frac{\mathrm{d}y_{cj+1}(\tau)}{\mathrm{d}\tau}\\
&\quad + \delta_{jN}\chi\mu(1-f_t)u\frac{\mathrm{d}y_{cN}(\tau)}{\mathrm{d}\tau} - \delta_{j1}\chi\mu(1-f_n)l_1 u\frac{\mathrm{d}\alpha_1(\tau)}{\mathrm{d}\tau} - \zeta_{\eta j}l_{j-1}\frac{\mathrm{d}\alpha_{j-1}(\tau)}{\mathrm{d}\tau}\\
&\quad + \{-\beta\zeta_{fj} + \beta\zeta_{bj} - \zeta_{\eta j} + \zeta_{\eta j+1} + 2\chi\mu u\}l_j\frac{\mathrm{d}\alpha_j(\tau)}{\mathrm{d}\tau} + \zeta_{\eta j+1}l_{j+1}\frac{\mathrm{d}\alpha_{j+1}(\tau)}{\mathrm{d}\tau}\\
&\quad + \delta_{jN}\chi\mu(1-f_t)l_N u\frac{\mathrm{d}\alpha_N(\tau)}{\mathrm{d}\tau} - \overline{k}_{\eta j}y_{cj-1}(\tau) + (\overline{k}_{fj} + \overline{k}_{bj} + \overline{k}_{\eta j} + \overline{k}_{\eta j+1})y_{cj}(\tau)\\
&\quad - \overline{k}_{\eta j+1}y_{cj+1}(\tau) + \delta_{j1}\chi\mu(1-f_n)u^2\alpha_1(\tau) - \overline{k}_{\eta j}l_{j-1}\alpha_{j-1}(\tau)\\
&\quad + l_j\left[(-\beta\overline{k}_{fj} + \beta\overline{k}_{bj} - \overline{k}_{\eta j} + \overline{k}_{\eta j+1}) - \frac{2\mu u^2}{\pi}\left\{\left(1 - \frac{\varepsilon - 1}{r_h}\right)C_T - C_N\right\}\right]\alpha_j(\tau)\\
&\quad + \overline{k}_{\eta j+1}l_{j+1}\alpha_{j+1}(\tau) + \delta_{jN}\mu\left\{\chi(1-f_t) - \frac{2C_b}{\pi}\right\}u^2\alpha_N(\tau) = 0,
\end{aligned} \tag{25}$$

$$\begin{aligned}
&2l_j\left\{\frac{1}{4} + \frac{l_j^2}{3} + \frac{1}{3}\chi\mu l_j^2\right\}\frac{\mathrm{d}^2\alpha_j(\tau)}{\mathrm{d}\tau^2} - \delta_{j1}\chi\mu(1-f_n)l_1 u\frac{\mathrm{d}y_{c1}(\tau)}{\mathrm{d}\tau} + \zeta_{\eta j}l_j\frac{\mathrm{d}y_{cj-1}(\tau)}{\mathrm{d}\tau}\\
&\quad + \{(-\beta\zeta_{fj} + \beta\zeta_{bj} - \zeta_{\eta j} + \zeta_{\eta j+1}) - 2\chi\mu u\}l_j\frac{\mathrm{d}y_{cj}(\tau)}{\mathrm{d}\tau} - \zeta_{\eta j+1}l_j\frac{\mathrm{d}y_{cj+1}(\tau)}{\mathrm{d}\tau}\\
&\quad + \delta_{jN}\chi\mu(1-f_t)l_N u\frac{\mathrm{d}y_{cN}(\tau)}{\mathrm{d}\tau} + \delta_{j1}\chi\mu(1-f_n)l_1^2 u\frac{\mathrm{d}\alpha_1(\tau)}{\mathrm{d}\tau} + (-\zeta_{\alpha j} + \zeta_{\eta j}l_{j-1}l_j)\frac{\mathrm{d}\alpha_{j-1}(\tau)}{\mathrm{d}\tau}\\
&\quad + \left\{(\beta^2\zeta_{fj} + \beta^2\zeta_{bj} + \zeta_{\eta j} + \zeta_{\eta j+1})l_j^2 + \zeta_{\alpha j} + \zeta_{\alpha j+1} + \frac{2\mu l_j^3}{3\pi}(uC_N + c)\right\}\frac{\mathrm{d}\alpha_j(\tau)}{\mathrm{d}\tau}\\
&\quad + (-\zeta_{\alpha j+1} + \zeta_{\eta j+1}l_j l_{j+1})\frac{\mathrm{d}\alpha_{j+1}(\tau)}{\mathrm{d}\tau} + \delta_{jN}\chi\mu(1-f_t)l_N^2 u\frac{\mathrm{d}\alpha_N(\tau)}{\mathrm{d}\tau} + \overline{k}_{\eta j}l_j y_{cj-1}(\tau)\\
&\quad + (-\beta\overline{k}_{fj} + \beta\overline{k}_{bj} - \overline{k}_{\eta j} + \overline{k}_{\eta j+1})l_j y_{cj}(\tau) - \overline{k}_{\eta j+1}l_j y_{cj+1}(\tau) - \delta_{j1}\chi\mu(1-f_n)l_1 u^2\alpha_1(\tau)\\
&\quad + (-\overline{k}_{\alpha j} + \overline{k}_{\eta j}l_{j-1}l_j)\alpha_{j-1}(\tau) + \{(\beta^2\overline{k}_{fj} + \beta^2\overline{k}_{bj} + \overline{k}_{\eta j} + \overline{k}_{\eta j+1})l_j^2 + \overline{k}_{\alpha j} + \overline{k}_{\alpha j+1} - 2\chi\mu l_j u^2\}\alpha_j(\tau)\\
&\quad + (-\overline{k}_{\alpha j+1} + \overline{k}_{\eta j+1}l_j l_{j+1})\alpha_{j+1}(\tau) + \delta_{jN}\mu\left\{\chi(1-f_t) - \frac{2C_b}{\pi}\right\}l_N u^2\alpha_N(\tau) = 0,
\end{aligned} \tag{26}$$

for $j = 1$ to N.

The dimensionless linearized equations of motion are rewritten in matrix form

$$[M]\left\{\begin{matrix}\ddot{y}\\ \ddot{\alpha}\end{matrix}\right\} + [C]\left\{\begin{matrix}\dot{y}\\ \dot{\alpha}\end{matrix}\right\} + [K]\left\{\begin{matrix}y\\ \alpha\end{matrix}\right\} = \{0\}, \tag{27}$$

where $[M]$ is the mass, $[C]$ the damping, and $[K]$ the stiffness matrix; $\{y|\alpha\}^{\mathrm{T}} = \{y_1, \alpha_1, y_2, \alpha_2, \ldots, y_N, \alpha_N\}^{\mathrm{T}}$ is the vector of the generalized coordinates. Solutions are then sought of the form

$$\left\{\frac{y}{\alpha}\right\} = \left\{\frac{\bar{y}}{\bar{\alpha}}\right\} \exp(\mathrm{i}\omega t) = \left\{\frac{\bar{y}}{\bar{\alpha}}\right\} \exp(\lambda t); \tag{28}$$

substituting into the previous equation we obtain

$$(\lambda[I] - [Y])\{\bar{\phi}_j\} = \{0\}, \tag{29}$$

in which $\lambda = \mathrm{i}\omega$; nontrivial solutions are obtained when $\det(\lambda[I] - [Y]) = 0$, which gives $2N$ eigenvalues of the matrix $[Y]$, λ_j. The eigenvalues λ_j of the system, which are generally complex, permit the assessment of (linear) stability for each set of system parameters. For a stable system, the λ_j are either real and negative or complex conjugate pairs with negative real parts. The corresponding eigenvectors are $\{\bar{\phi}_j\}$.

Critical values of any given system parameter, in our case the flow velocity u, are associated with the state of neutral stability of the system, where the eigenvalues of the linearized system contain a purely imaginary pair or a single zero value. When the critical values are surpassed, the system becomes unstable.

3. Conversion of the discrete system into a continuous one, and comparison with previous work

3.1. Conversion of the discrete model into a continuous Timoshenko-beam model

The relationship for stiffness of the discrete and continuous systems is given next. The moment and shear forces acting on an element of the continuous model are given by

$$M = \frac{EI}{\rho_r}, \quad Q = k'AG\phi,$$

where ρ_r is the radius of curvature, A the cross-sectional area, E Young's modulus, I the second moment of the cross-sectional area, and $k'G$ the effective shear modulus. Those of the discrete model are

$$M = k_\alpha \alpha, \quad Q = k_\eta l_c^* \phi,$$

where $l_c^* (= 2l^*)$ is the length of each car. By letting the moment and shear forces of the continuous system be equal those of the discrete one, we obtain

$$k_\alpha = \frac{EI}{\rho_r \alpha} = \frac{EI}{l_c^*}, \quad k_\eta = \frac{k'AG}{l_c^*}. \tag{30}$$

Accordingly, the rotational and translational springs, k_α and k_η, interconnecting the cars are related to the flexural and shear rigidity of the continuous system by Eqs. (30).

Next, based on these relationships, we convert the present discrete system of the train of cars into a continuous system. Initially, for the sake of clarity, the dimensionless equations of motion of the train, Eqs. (25) and (26), are simplified by (i) omitting all the (mechanical) dampers, (ii) omitting the terms for the leading ($j = 1$) and trailing ($j = N$) cars for the infinite-length system, and (iii) letting $\overline{k}_{fj} = \overline{k}_{bj} = 0$, $\overline{k}_{\eta j} = \overline{k}_{\eta j+1} = \overline{k}_\eta$, $\overline{k}_{\alpha j} = \overline{k}_{\alpha j+1} = \overline{k}_\alpha$, and $l_{j-1} = l_j = l_{j+1} = l$ in the dimensionless equations of motion for the jth car. The simplified equations are given by

$$m_j \ddot{y}_{cj}^*(t) - k_\eta\{y_{cj+1}^*(t) - 2y_{cj}^*(t) + y_{cj-1}^*(t)\} + k_\eta l^*\{\alpha_{j+1}(t) - \alpha_{j-1}(t)\} = 0, \tag{31}$$

$$J_c \ddot{\alpha}_j(t) - k_\eta l^*\{y_{cj+1}^*(t) - y_{cj-1}^*(t)\} + (-k_\alpha + k_\eta l^{*2})\{\alpha_{j+1}(t) - 2\alpha_j(t) + \alpha_{j-1}(t)\} = 0. \tag{32}$$

Introducing difference equations,

$$\frac{\partial y_{cj}}{\partial x} = \frac{y_{cj+1} - y_{cj-1}}{2l_c^*}, \quad \frac{\partial^2 y_{cj}}{\partial x^2} = \frac{y_{cj+1} - 2y_{cj} + y_{cj-1}}{l_c^{*2}},$$

$$\frac{\partial \alpha_j}{\partial x} = \frac{\alpha_{j+1} - \alpha_{j-1}}{2l_c^*}, \quad \frac{\partial^2 \alpha_j}{\partial x^2} = \frac{\alpha_{j+1} - 2\alpha_j + \alpha_{j-1}}{l_c^{*2}},$$

and substituting the difference equations into the simplified equations of motion, and then making use of Eq. (30), we have

$$\frac{k'G}{\rho_c}\left(\frac{\partial^2 y^*_{cj}}{\partial x^2}-\frac{\partial \alpha_j}{\partial x}\right)=\frac{\partial^2 y^*_{cj}}{\partial t^2},\quad \left(\frac{EIl^*_c}{J_c}-\frac{k'AGl^{*3}_c}{4J_c}\right)\frac{\partial^2 \alpha_j}{\partial x^2}+\frac{k'AGl^*_c}{J_c}\left(\frac{\partial y_{cj}}{\partial x}-\alpha_j\right)=\frac{\partial^2 \alpha_j}{\partial t^2}.$$

Furthermore, if $l^{*2}_c \ll a^2$, the mass-moment of inertia of a car about the centre of mass, J_c can be related to the second moment of area I as

$$J_c=\rho_c A l^*_c\left(\frac{a^2}{4}+\frac{l^{*2}_c}{12}\right)\simeq \rho_c A l^*_c\left(\frac{a^2}{4}\right)=\rho_c l^*_c\left(\frac{\pi a^4}{4}\right)=\rho_c l^*_c I.$$

Finally, the discrete system is converted to a continuous one by letting $l^*_c \to 0$, $y_{cj} \to y$, and $\alpha_j \to \alpha$. This gives

$$a_1^2\left(\frac{\partial^2 y^*}{\partial x^2}-\frac{\partial \alpha}{\partial x}\right)=\frac{\partial^2 y^*}{\partial t^2}, \tag{33}$$

$$a_2^2\frac{\partial^2 \alpha}{\partial x^2}+a_1^2\kappa^2\left(\frac{\partial y^*}{\partial x}-\alpha_j\right)=\frac{\partial^2 \alpha}{\partial t^2}, \tag{34}$$

where the following abbreviations have been introduced:

$$\frac{E}{\rho}=a_2^2,\quad \frac{k'G}{\rho}=a_1^2,\quad \frac{A}{I}=\kappa^2. \tag{35}$$

Eqs. (33) and (34) are in the form of the transverse and rotational direction equations of motion, respectively, for a continuous Timoshenko beam (Crandall et al., 1968). Hence, it has been demonstrated that the present model of the train of cars can be considered as a lumped-parameter Timoshenko-beam (LTB) model.

A significant feature of this system of flexibly interconnected cars is that, unlike a Timoshenko beam in which the flexural and shear rigidities are interrelated in terms of the material properties, in this case flexural and shear rigidities are related to different sets of springs; hence, by altering the values of these springs, the equivalent Timoshenko model can be made to approach the Euler–Bernoulli model (instead of doing so by slenderness considerations).

3.2. Comparisons with previous work for the continuous Euler–Bernoulli beam

Here, in order to obtain the equivalent continuous Euler–Bernoulli beam system, the Timoshenko beam effects of rotational inertia and shear deformation will be neglected. Neglecting the rotational inertia effect implies that the mass-moment of inertia is set to zero ($J \to 0$). To neglect the shear deformation effect, the translational springs interconnecting the cars are given very large values (i.e. $k_\eta \to \infty$), so that the cars cannot undergo lateral translational motion. In fact, letting $J \to 0$ and $k_\eta \to \infty$ (i.e. $G \to \infty$, see Eq. (30)) in the Timoshenko equation (Thomson, 1993),

$$EI\frac{\partial^4 y}{\partial x^4}+m\frac{\partial^2 y}{\partial t^2}-\left(J+\frac{EIm}{kAG}\right)\frac{\partial^4 y}{\partial x^2\partial t^2}+\frac{Jm}{kAG}\frac{\partial^4 y}{\partial t^4}=p(x,t)+\frac{J}{kAG}\frac{\partial^2 p}{\partial t^2}-\frac{EI}{kAG}\frac{\partial^2 p}{\partial x^2}, \tag{36}$$

we obtain the Euler–Bernoulli equation

$$EI\frac{\partial^4 y}{\partial x^4}+m\frac{\partial^2 y}{\partial t^2}=p(x,t). \tag{37}$$

In addition, we employ the relation $k_\alpha = EI/l^*_c$ derived in Section 3.1. We undertake a comparison between the present model and the pinned–pinned continuous Euler–Bernoulli beam, because a certain amount of work for pinned–pinned continuous systems has been studied in the past. The values of the variables in the present model are chosen the same as in the previous work in order to reduce it to the equivalent continuous Euler–Bernoulli beam model.

The dynamical behaviour of the articulated system ($N = 5$) and of the continuous system with increasing flow velocity is shown in Fig. 5. A set of parameters for the articulated system in Fig. 5 is given in Table 1. The results of the continuous system are from Païdoussis (1973). The real and imaginary parts of the lowest two eigenvalues of the system, $\mathrm{Re}(\lambda)$ and $\mathrm{Im}(\lambda)$, which are proportional to the damping and frequency of the oscillation, respectively, are plotted in the form of an Argand diagram. With increasing flow velocity, starting from 0 m/s, free oscillations of the first and second modes of both systems are damped. As shown in Fig. 5, at $U \simeq 3.14$ m/s for the articulated system, and at $U \simeq 3.27$ m/s for the continuous system, the frequencies of the first mode become purely real, bifurcating on the $\mathrm{Re}(\lambda)$-axis.

The first branch of the first mode of the articulated system goes through the origin ($\mathrm{Re}(\lambda)>0$) at a U slightly higher than $U \simeq 3.14\,\mathrm{m/s}$, indicating buckling; the same occurs for the second branch, at $U \simeq 5.89\,\mathrm{m/s}$. Then, for a very slight increase in U, the two branches coalesce and leave the $\mathrm{Re}(\lambda)$-axis at the point where $\mathrm{Re}(\lambda)>0$, indicating the onset of coupled-mode flutter. On the other hand, the eigenvalues of the second modes of the discrete and the continuous systems never take positive $\mathrm{Re}(\lambda)$ values. Their behaviour demonstrates that the second mode in both systems always remains stable. Note that the critical flow velocities of the discrete system are lower than those of the continuous one (e.g., $3.14\,\mathrm{m/s}<3.27\,\mathrm{m/s}$, $5.89\,\mathrm{m/s}<6.55\,\mathrm{m/s}$, etc.). Nevertheless, although the loci of the continuous and articulated systems display some differences in both modes, the dynamical behaviour of the articulated system is in sensibly good agreement with that of the continuous one.

Moreover, it has been shown that the present model is in good agreement with previous results for pinned–pinned continuous systems, which further verifies the methodology of the present model. In addition, the present Lumped-Parameter Timoshenko Beam (LTB) model can replicate the dynamical behaviour of a continuous Euler–Bernoulli beam under certain conditions (Sakuma, 2006). Also, because it was shown that the overall dynamical behaviour of the *lumped-parameter* Euler–Bernoulli (LEB) model and that of the *continuous* Euler–Bernoulli model subjected to fluid dynamic forces are similar to each other (Païdoussis, 1986), the LTB model can replicate the dynamical behaviour of the LEB model (Sakuma, 2006).

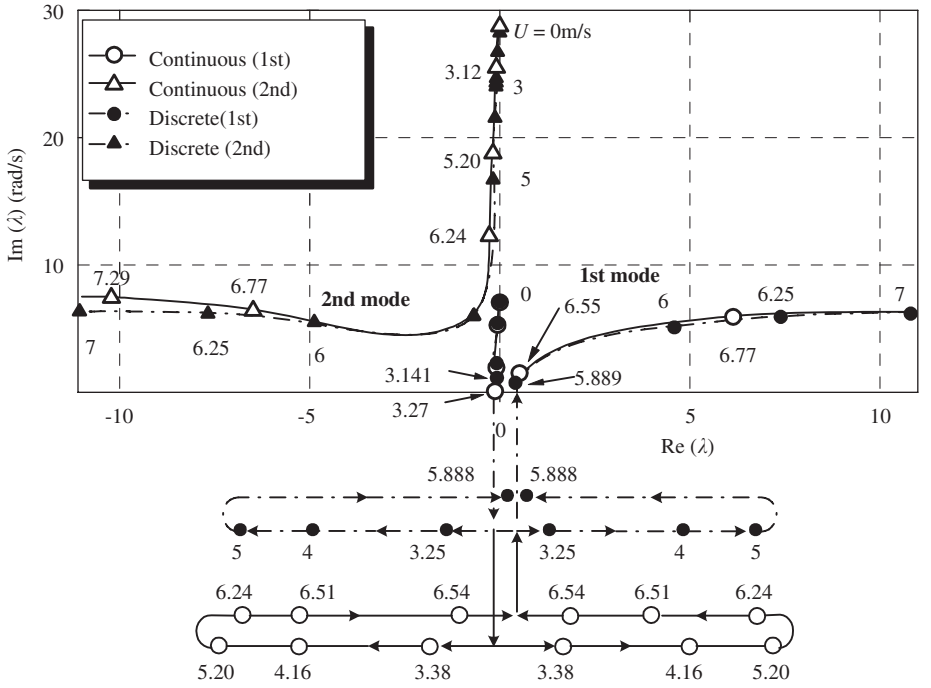

Fig. 5. Argand diagram of the pinned–pinned continuous system and that of the articulated system ($N = 5$) with increasing flow velocity. The loci on the $\mathrm{Re}(\lambda)$-axis are shown separately below for clarity. The results of the continuous system are from Païdoussis (1973).

Table 1
System parameters for the pinned–pinned articulated system shown in Fig. 5

$N = 5$	$l_1 = l_5 = 6.25$ (0.0625 m)	$l_2 = l_3 = l_4 = 12.5$ (0.125 m)
$L_A = 100$ (1.0 m)	$a = 0.01$ m	$R^*/a = 1000$
$\rho = 1000\,\mathrm{kg/m^3}$	$\rho_{\mathrm{car}} = 1083\,\mathrm{kg/m^3}$	$C_N = C_T = 0.0039$
$C_D = C_b = 0$	$f_n = f_t = 0$	$k_f = k_b = 0$
$k_\alpha = 1.36\,\mathrm{N\,m/rad}$	$k_\eta = 1.0 \times 10^8\,\mathrm{N/m}$	Zero mechanical damping

L_A is dimensionless total length of train.

4. Dynamics of the train system modelled as a Lumped-parameter Timoshenko Beam (LTB)

In this section, the critical flow velocities for neutral stability and corresponding frequencies associated with instabilities of the train-like system are calculated systematically, demonstrating the effect of the various parameters on the stability of the system. The tested dimensionless parameters are the mass ratio, number of cars or cylindrical bodies, blockage ratio, spring coefficients, damping coefficients, frictional drag coefficients in the normal and longitudinal directions, streamlining coefficient at the nose of the train, base drag coefficient with streamlining coefficient at the tail of the train, zero-flow normal coefficient, and ratio of cross-sectional area of hood to that of the cars. Since the instability appears to occur first in either the first or second modes, the conditions of stability associated only with these two modes are considered.

For a given set of system parameters and for each mode, the values of u and $\mathrm{Im}(\lambda)$ at the point of neutral stability, where $\mathrm{Re}(\lambda)=0$, were determined by the method given in Section 2. The flow velocity is varied up to $\simeq 300\,\mathrm{m/s}$. In addition to the dimensionless critical flow velocities, the percentage difference between the critical flow velocity obtained with a set of parameters and the value obtained for a set of "standard" system parameters are given. This enables the effect of the various system parameters on the stability of the system to be evaluated. A set of typical parameters for an actual high-speed train is mainly employed as the "standard," as given in Table 2 (Fujimoto, 1999; Manabe, 2002). In the simulations presented in the following, the percentage differences are calculated as $100(u_{cr}-u_{cr}^{sd})/u_{cr}^{sd}$, where u_{cr} is the critical flow velocity for the particular parameters used and u_{cr}^{sd} is that for the "standard", reference system.

First, to understand the typical dynamical behaviour of the system, Argand diagrams of the lowest three dimensionless frequencies for $N=4$ and 8 are given in Fig. 6(a). It is seen that small flow velocities act to damp free oscillations of the system. As the flow velocity is increased, however, the system becomes unstable by flutter in the first mode for $N=4$ at $u=9.1$, and in both the first and second modes for $N=8$ at $u=8.0$ and 9.3, respectively, where those loci eventually cross the $\mathrm{Im}(\lambda)$-axis. From the examples in Fig. 6(a), the typical dynamical behaviour may be summarized as follows: small flow velocities act to damp free oscillations of the system; and then, as the flow velocity increases, the system becomes unstable by flutter in its lower modes.

The effect of the number of cars on the dynamics is examined in more detail. The number of cars in the train is varied from $N=4$ to 16 and the results are shown in Fig. 6(b). The dimensionless critical flow velocities of the first and second modes and the percentage differences with the "standard" system ($N=8$) are shown in the figure. As the number of cars increases, the dimensionless critical velocities of the first and second modes decrease. Note that there are no critical flow velocities for the second mode if $N<8$ (cf. Fig. 6(a)). The percentage difference between the critical velocities for $N=4$ and 16 is about 28%, as shown in Fig. 6(b).

Next, the effect of the frictional drag coefficients in the normal and longitudinal directions, C_N and C_T, is examined. The ratio of the frictional drag coefficients in the normal and longitudinal directions is varied from $C_N/C_T=0.25$ to 1.0. The value of C_N is fixed at 0.0126 and that of C_T is changed. Note that we obtained almost the same results if the value of C_T was fixed and that of C_N was changed. Argand diagrams of the lowest three dimensionless frequencies for $C_N/C_T=0.25$, 0.50, 0.75, and 1.0 are illustrated in Fig. 7(a). It is shown that for all the cases considered small flow velocities act to damp free oscillations of the system. As the flow velocity increases, however, the system becomes unstable by flutter in all three modes for $C_N/C_T=0.25$, in both the first and second modes for $C_N/C_T=0.5$ ($u_{cr1}=8.0, u_{cr2}=9.3$), and in only the first mode for $C_N/C_T=0.75$ ($u_{cr1}=10.0$). On the other hand, no instability occurs for $C_N/C_T=1.0$; cf. Païdoussis (2003, Section 8.3.3). It should be noted that Païdoussis (2003) reviewed papers for cylinders in axial flow and suggests the range of the ratio of C_N/C_T as $0.5\leqslant C_N/C_T\leqslant 1.6$.

Table 2
System parameters for a finite-length train of the LTB model in a tunnel

$N=8$	$2l_j\ (=l_{\mathrm{car}})=14.12\ (25\,\mathrm{m})$	$L_A=113.0\ (200\,\mathrm{m})$
$a=1.77\,\mathrm{m}$	$\beta=0.72$	$R^*/a=2.24$
$A/A_d=0.2$	$A'/A=1.0$	$\rho=1.23\,\mathrm{kg/m^3}$
$\rho_{\mathrm{car}}=151.6\,\mathrm{kg/m^3}$	$C_N=0.0126$	$C_T=2C_N=0.0252$
$C_D=0.0126$	$C_b=0.157$	$f_n=1.0$
$f_t=0.8$	$k_f=k_b=353\,000\,\mathrm{N/m}\ (=k_0)$	$k_\alpha=0\,\mathrm{N\,m/rad}$
$k_\eta=9800\,\mathrm{N/m}$	Zero mechanical damping	

A_d is cross-sectional area of a duct (tunnel).

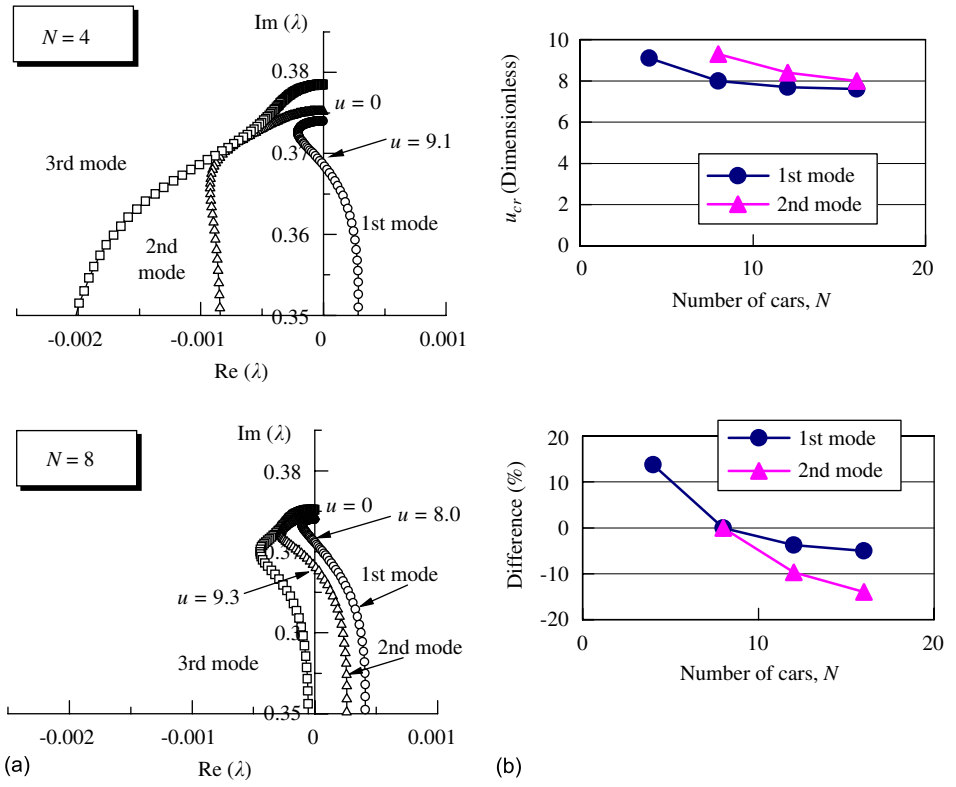

Fig. 6. (a) Argand diagrams for $N = 4$ and 8. (b) Effect of number of cars on the dynamics of the system. The percentage difference is defined in Section 4.

However, as suggested by Ortloff and Ives (1969), $C_N/C_T = 0.5$ is appropriate for hydrodynamically very rough cylinders, and a real train (with all its protrusions) must not be far off that.

The critical flow velocities and the percentage differences as C_N/C_T is varied are given in Fig. 7(b). The dimensionless critical velocities of the first and second modes increase with increasing the C_N/C_T ratio. The critical velocities for the second mode do not exist for $C_N/C_T > 0.5$, and those for the first mode do not exist for $C_N/C_T > 0.75$. In other words, if C_T is about 30% larger than C_N ($C_N/C_T \leqslant 0.75$ or $C_T/C_N \geqslant 1.3$), the loci cross the Im(λ)-axis, and thus, the system becomes unstable. The system becomes more unstable as C_T becomes larger than C_N. The percentage difference between the critical velocities for $C_N/C_T = 0.25$ and 0.75 is about 50%, as shown in Fig. 7(b).

In the same manner, the other parameters are examined. The results are summarized in Table 3. The values of "Range" in Table 3 can be either the values of the parameter or a multiplication factor, as denoted in the previous sections, and "[none]" means that the critical velocity does not exist at the upper-end value of the range. E.g., for μ, the range is 0.5–4.0; for k_f (and k_b), 0.01–3.0; for k_η, $k_\eta = 0.01$–100; and for k_α, $k_\alpha = 0$–1. From these results it is apparent that the mass ratio, blockage ratio, spring and damping coefficients, and frictional drag coefficients have considerable effect on the stability of the system.

The effect of varying C_N/C_T has a larger effect on the dynamics ($\geqslant 50\%$) than any of the other aerodynamic parameters, f_n, f_t, C_b, C_D, and ε ($\leqslant 25\%$), as shown in Table 3.

It is recalled that the stability of similar models of articulated cylinders subjected to axial flow depends strongly on the parameter f_t (Païdoussis, 1966a, 1973). The main reason why f_t has a small effect here, while in Païdoussis' work it had a large effect, is that the two systems are quite different: LTB systems are studied here, while in Païdoussis' work it is an LEB system. An essential difference in the conditions for positive work done by the fluid on the articulated systems of the LEB and LTB models is that for the LEB model, the motion of all the cars has to be considered simultaneously; while for the LTB model, the motion of each car is considered separately. This may appear to be a superficial difference; however, as will be seen in the next section, it has repercussions on the mechanisms of instability of the two types of model.

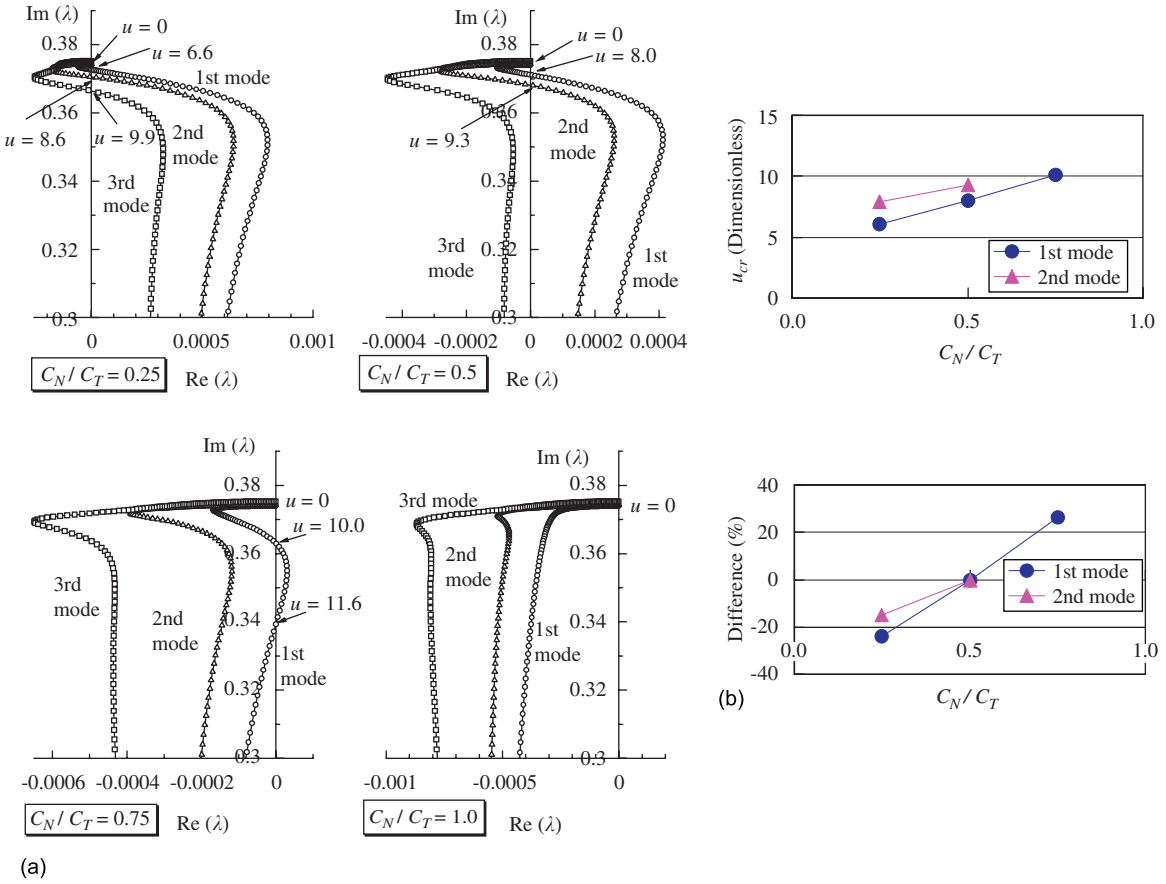

Fig. 7. (a) Argand diagrams for varying from $C_N/C_T = 0.25$ to 1.0. (b) Effect of viscous frictional drag coefficients in the normal and longitudinal directions on the dynamics of the system. The value of C_N is fixed at 0.0126 and that of C_T is changed. The percentage difference is defined in Section 4.

5. The mechanism of instability for the Lumped-parameter Euler–Bernoulli (LEB) and Timoshenko Beam (LTB) models

The mechanisms of instability for the LEB and LTB models and their differences are the topic of this section. As mentioned in the Introduction, in some studies, actual train sets have been modelled as Euler–Bernoulli beams, where rotational inertia and shear deformation are neglected. Since the vehicles of actual trains have rotational inertia and adjacent cars can have different translational (transverse) motion, corresponding to shear deformation of a beam, both effects need to be included in the model. Hence, it is preferable that an actual train be modelled as a Timoshenko beam. Here, the mechanism of instability of the LEB and LTB models is clarified with the aid of the computed modal shapes and the work done by the fluid on the system.

Although the train is best modelled as a free–free system, as considerable previous work exists for the cantilevered system, a cantilever model will also be considered in this paper as a reference case.

The rate at which the fluid does work on the train is given by (Benjamin, 1961)

$$\frac{\mathrm{d}W}{\mathrm{d}t} = Q_1\dot{q}_1 + Q_2\dot{q}_2 + \cdots + Q_n\dot{q}_n, \tag{38}$$

where $q_j (j = 1, 2, \ldots, n)$ are the generalized coordinates and Q_j the generalized force components representing the action of the fluid. The generalized fluid forces are given by letting all the terms related to mechanical masses, dampers, and springs in the equations of motion be equal to zero.

Table 3
Variations in critical velocity with respect to system parameters for a finite-length train modelled as a LTB system in a tunnel

Parameter	Nomenclature	Range	Difference (±%)
Number of cars	N	4–16	−28
Mass ratio	μ	0.5–4.0	−91
Blockage ratio	A/A_d	0.001–0.7	−64
Spring coefficients	Translational to wall $\overline{k}_f, \overline{k}_b$	0.01–3.0	+154 [none]
	Translational to cars $\overline{k}_\eta$	0.01–100	+28
	Rotational to cars $\overline{k}_\alpha$	0–1.0	+16 [none]
Damping coefficients	Translational to wall c_f, c_b	0–80 (N s/m)	+16 [none]
	Tanslational to cars c_η	$0-4\times10^3$ (N s/m)	+6 [none]
	Rotational to cars c_α	$0-3\times10^4$ (N m s/rad)	+6 [none]
Frictional drag coefficients	C_N/C_T (C_N: fixed)	0.25–0.75	+50 [none]
Form drag coefficient	c_b (or $C_b=(1-f_t)\pi/4$)	0–0.1–1.0	$-21\rightarrow3\rightarrow-11$
Streamlining coefficient	Front f_n	0–0.91–1.0	$10\rightarrow20\rightarrow0$
	Tail f_t	0–0.9–1.0	$-11\rightarrow3\rightarrow-21$
Zero-flow normal coefficient	C_D	1–10	+1
Ratio of cross-sectional area of hood to that of car	$\varepsilon=A'/A$	0–1.0	+25

"Range" means either the value of a parameter or the multiplication factor; "[none]" means that the critical velocity does not exist at the upper-end values of the ranges. The percentage difference is defined in Section 4.

The work done ΔW on the system can generally be obtained by integrating Eq. (38) over a period of oscillation, T, as

$$\Delta W=\int_0^T (Q_1\dot{q}_1+Q_2\dot{q}_2+\cdots+Q_n\dot{q}_n)\,\mathrm{d}t. \tag{39}$$

5.1. LEB model

The modified equations of motion of a free–free system in unconfined space—for the case when the mass of the car, m_c, and that of fluid, m_f, are different, instead of $m=m_c=m_f$ as in Païdoussis (1986), are given by

$$\begin{aligned}
&(m_c+m_f)sl\ddot{y}+(m_c+m_f)l^2\sum_{j=1}^{N}c_j\sum_{k=1}^{j-1}c_k\ddot{\theta}_k+\frac{1}{2}(m_c+m_f)l^2\sum_{j=1}^{N}c_j^2\ddot{\theta}_j\\
&\quad+m_fUl\sum_{j=1}^{N}c_j\dot{\theta}_j+\frac{1}{2}c_N\left(\frac{m_f}{D}\right)U\left\{sl\dot{y}+l^2\sum_{j=1}^{N}c_j\sum_{k=1}^{j-1}c_k\dot{\theta}_k+\frac{1}{2}l^2\sum_{j=1}^{N}c_j^2\dot{\theta}_j+Ul\sum_{j=1}^{N}c_j\theta_j\right\}\\
&\quad-\frac{1}{2}c_T\left(\frac{m_f}{D}\right)U^2l\sum_{j=1}^{N}c_j\theta_j+(1-f_t)m_fU\left[\dot{y}+l\sum_{j=1}^{N}c_j\dot{\theta}_j+U\theta_N\right]\\
&\quad+(1-f_n)m_fU(\dot{y}+U\theta_1)-\frac{1}{2}c_Dm_fU^2\theta_N+\frac{1}{2}m_fU^2\left[c_D+c_T\left(\frac{s}{D}\right)l\right]\theta_1=0,
\end{aligned} \tag{40}$$

where $s=\sum_{j=1}^{N}c_j$, $c_N=(4/\pi)C_N$, $c_T=(4/\pi)C_T$ and $c_D=(4\pi)C_b$ and

$$\begin{aligned}
&(m_c+m_f)l^2\sum_{j=1}^{N}c_j\left\{\sum_{k=1}^{j-1}c_k\delta_{km}+\frac{1}{2}c_j\delta_{jm}\right\}\left\{\ddot{y}+l\sum_{k=1}^{j-1}c_k\ddot{\theta}_k\right\}\\
&\quad+(m_c+m_f)l^3\sum_{j=1}^{N}c_j^2\left\{\frac{1}{2}\sum_{k=1}^{j-1}c_k\delta_{km}+\frac{1}{3}c_j\delta_{jm}\right\}\ddot{\theta}_j+m_fUl^2\sum_{j=1}^{N}c_j\left\{\sum_{k=1}^{j-1}c_k\delta_{km}+\frac{1}{2}c_j\delta_{jm}\right\}\dot{\theta}_j
\end{aligned}$$

$$- m_f U l c_m \dot{y} - m_f U l^2 \sum_{j=1}^{N} c_j \delta_{jm} \sum_{k=1}^{j-1} c_k \dot{\theta}_k - \frac{1}{2} m_f U l^2 \sum_{j=1}^{N} \delta_{jm} c_j^2 \dot{\theta}_j - m_f U^2 l \sum_{j=1}^{N} \delta_{jm} c_j \theta_j + K_\alpha \sum_{j=1}^{N} (\theta_{j+1} - \theta_j)(\delta_{j+1,m} - \delta_{jm}) - Q_m = 0, \tag{41}$$

where $m = 1, \ldots, N$, and

$$\begin{aligned} Q_m = & -\frac{1}{2} c_N \left(\frac{m_f}{D}\right) U \left[\frac{1}{2} c_m^2 l^2 \left\{ \dot{y} + l \sum_{k=1}^{m-1} c_k \dot{\theta}_k \right\} + \frac{1}{3} c_m^3 l^3 \dot{\theta}_m + \frac{1}{2} c_m^2 l^2 U \theta_m \right] \\ & + \sum_{j=m+1}^{N} \left[-\frac{1}{2} c_N \left(\frac{m_f}{D}\right) U c_m l \left\{ \left(\dot{y} + l \sum_{k=1}^{j-1} c_k \dot{\theta}_k \right) c_j l + \frac{1}{2} c_j^2 l^2 \dot{\theta}_j + U c_j l \theta_j \right\} \right] \\ & + \sum_{j=m+1}^{N} \left\{ \frac{1}{2} c_T \left(\frac{m_f}{D}\right) U^2 c_j c_m l^2 (\theta_j - \theta_m) \right\} + \frac{1}{2} c_D \rho A U^2 c_m l (\theta_N - \theta_m) \\ & - (1 - f_t) \rho A U c_m l \left\{ \dot{y} + l \sum_{j=1}^{N} c_j \dot{\theta}_j + U \theta_N \right\}. \end{aligned} \tag{42}$$

Eq. (40) is the "y equation" and Eq. (41) is the "θ equation." The (y, θ) coordinate system of the LEB model is illustrated in Fig. 8(a). The work done ΔW for the LEB (free–free) system can be written by integrating Eq. (38) over a period of oscillation, T, as

$$\Delta W = \int_0^T (Q_y \dot{q}_y + Q_1 \dot{q}_1 + Q_2 \dot{q}_2 + \cdots + Q_N \dot{q}_N)\, \mathrm{d}t = \Delta W^y + \sum_{m=1}^{N} (\Delta W_m^\theta). \tag{43}$$

For reference, as considerable work already exists for such a system, we also consider a cantilevered (clamped–free) system, for which $y = 0$, and thus, $\Delta W_j^y = \int_0^T Q_y \dot{q}_y \, \mathrm{d}t = 0$. Then, we have

$$\Delta W = \int_0^T (Q_1 \dot{q}_1 + Q_2 \dot{q}_2 + \cdots + Q_N \dot{q}_N)\, \mathrm{d}t = \sum_{m=1}^{N} (\Delta W_m^\theta).$$

By letting all the terms related to mechanical masses m_c and springs K_α be zero and $y = 0$ in Eqs. (40)–(42), the work done for all cars in the clamped–free system over a period of oscillation, T, is given by

$$\begin{aligned} \Delta W^\theta = & \sum_{m=1}^{N} \Delta W_m^\theta = -m_f l^3 \left\{ \sum_{m=1}^{N} c_m \sum_{j=m+1}^{N} c_j \sum_{k=1}^{j-1} c_k \int_0^T \ddot{\theta}_k \dot{\theta}_m \, \mathrm{d}t + \frac{1}{2} \sum_{m=1}^{N} c_m^2 \sum_{k=1}^{m-1} c_k \int_0^T \ddot{\theta}_k \dot{\theta}_m \, \mathrm{d}t \right\} \\ & - \frac{1}{2} m_f l^3 \sum_{m=1}^{N} c_m \sum_{j=m+1}^{N} c_j^2 \int_0^T \ddot{\theta}_j \dot{\theta}_m \, \mathrm{d}t - m_f U l^2 \sum_{m=1}^{N} c_m \sum_{j=m+1}^{N} c_j \int_0^T \dot{\theta}_j \dot{\theta}_m \, \mathrm{d}t \\ & + m_f U l^2 \sum_{m=1}^{N} c_m \sum_{k=1}^{m-1} c_k \int_0^T \dot{\theta}_k \dot{\theta}_m \, \mathrm{d}t + \frac{1}{2} m_f U l^2 \sum_{m=1}^{N} c_m^2 \int_0^T \dot{\theta}_m^2 \, \mathrm{d}t \\ & - \frac{1}{4} c_N \left(\frac{m_f}{D}\right) U l^3 \sum_{m=1}^{N} c_m^2 \sum_{k=1}^{m-1} c_k \int_0^T \dot{\theta}_k \dot{\theta}_m \, \mathrm{d}t - \frac{1}{2} c_N \left(\frac{m_f}{D}\right) U l^3 \sum_{m=1}^{N} c_m \sum_{j=m+1}^{N} c_j \sum_{k=1}^{j-1} c_k \int_0^T \dot{\theta}_k \dot{\theta}_m \, \mathrm{d}t \\ & - \frac{1}{4} c_N \left(\frac{m_f}{D}\right) U l^3 \sum_{m=1}^{N} c_m \sum_{j=m+1}^{N} c_j^2 \int_0^T \dot{\theta}_j \dot{\theta}_m \, \mathrm{d}t + \frac{1}{2} (c_T - c_N) \left(\frac{m_f}{D}\right) U^2 l^2 \sum_{m=1}^{N} c_m \sum_{j=m+1}^{N} c_j \int_0^T \theta_j \dot{\theta}_m \, \mathrm{d}t \\ & - (1 - f_t) \rho A U \sum_{m=1}^{N} c_m \sum_{j=1}^{N} c_j l^2 \int_0^T \dot{\theta}_j \dot{\theta}_m \, \mathrm{d}t - \frac{1}{2} (1 - f_t) m_f U^2 l \sum_{m=1}^{N} c_m \int_0^T \theta_N \dot{\theta}_m \, \mathrm{d}t, \end{aligned} \tag{44}$$

where $c_b = 1 - f_t$ is assumed. Note that we omitted terms proportional to $\int_0^T \dot{\theta}_m^2 \, \mathrm{d}t$ with minus signs in Eq. (44) because they are always negative, and thus, these terms damp out the motions.

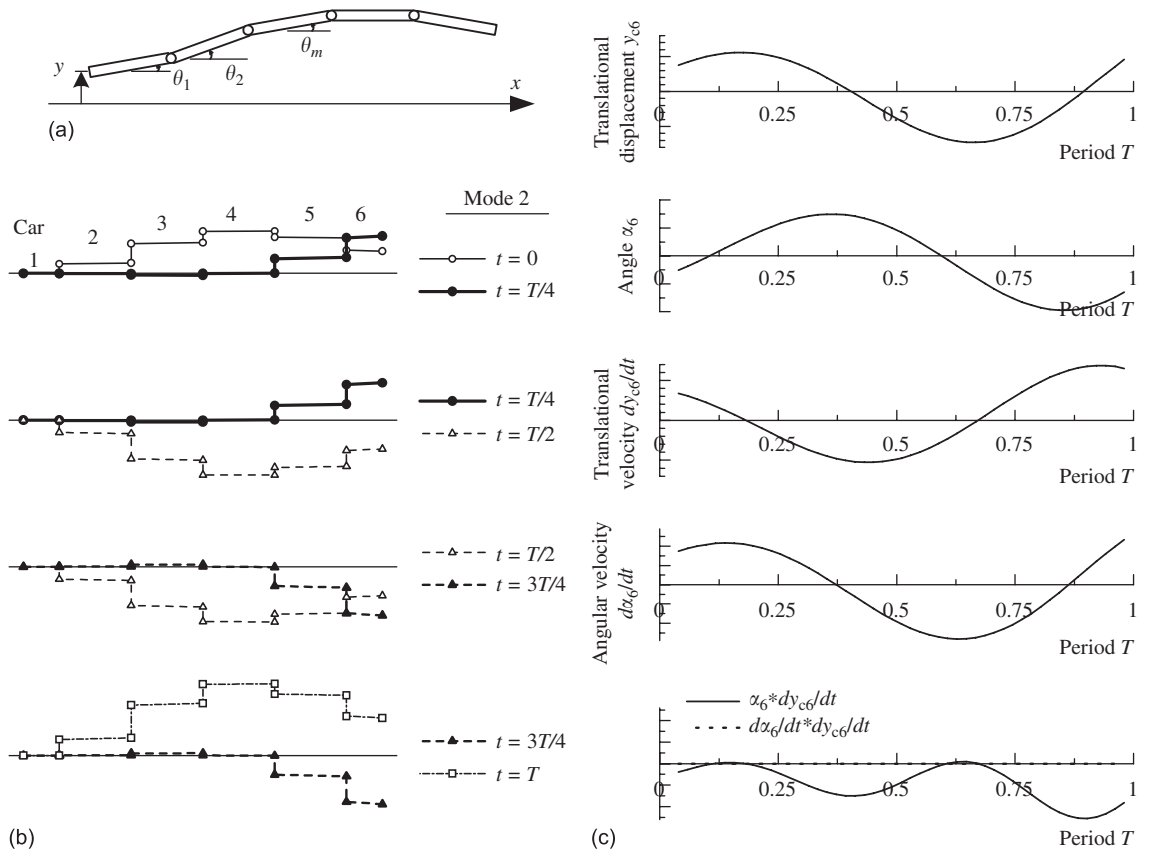

Fig. 8. (a) The (y,θ) coordinate system of a lumped parameter Euler–Bernoulli beam (LEB) model (Païdoussis, 1986). (b) Modal shapes of the lowest three eigenmodes of the clamped–free LTB model over a period of oscillation, $t = 0, T/4, T/2, 3T/4, T$ ($N = 6$, $f_t = 0.8$, $C_T = C_N$, $U = 4.49$ m/s). (c) Time histories of displacement, angle, the corresponding velocities, and their products for the trailing car, Car 6, for the clamped–free LTB model over a period of oscillation T ($N = 6$, $f_t = 0.8$, $C_T = C_N$, $U = 4.49$ m/s).

5.2. LTB model

In the same manner as for the LEB model, the work done for the LTB model can be obtained. Using Eqs. (25) and (26), letting all the terms related to mechanical masses, dampers, and springs be zero, assuming $C_b = (\pi/4)c_b = (\pi/4)(1-f_t)$, and letting $\chi \simeq 1$ and $1/r_h \simeq 0$ for $R^* \gg a$, corresponding to an unconfined fluid around the train, the work done for the LTB (free–free) system for the whole train over a period of oscillation, T, is given by

$$\Delta W = 2\mu(1-f_n)l_1 u\int_0^T \dot{\alpha}_1\dot{y}_{c1}d\tau - \mu(1-f_n)u^2\int_0^T \alpha_1\dot{y}_{c1}\,\mathrm{d}\tau + \frac{2\mu u^2}{\pi}(C_T - C_N)\sum_{j=1}^{N} l_j\int_0^T \alpha_j\dot{y}_{cj}\,\mathrm{d}\tau$$
$$- 2\mu(1-f_t)l_N u\int_0^T \dot{\alpha}_N\dot{y}_{cN}\,\mathrm{d}\tau - \frac{1}{2}\mu(1-f_t)u^2\int_0^T \alpha_N\dot{y}_{cN}\,\mathrm{d}\tau. \tag{45}$$

Note that, again, the terms of integrations of squared variables such as $\int_0^T \dot{y}_{cj}^{*2}\,\mathrm{d}t$ and $\int_0^T \dot{\alpha}_j^2\,\mathrm{d}t$ with minus signs are omitted because these terms are always negative, and thus, correspond to a loss in energy.

5.3. Conditions for positive work done by the fluid

As shown in Eqs. (44) and (45), the expressions for the work done consist of several terms related to fluid forces. To understand the contribution of each term to the mechanism of instability, conditions for positive work are summarized in a table with the aid of schematic drawings of the motion of the train cars.

We discuss the mechanism of instability considering only terms involving the flow velocity in Eqs. (44) and (45), because we know that the system becomes unstable as the flow velocity u increases. For instance, look at the first term of the right-hand side of Eq. (45), $2\mu(1-f_n)l_1u\int_0^T \dot{\alpha}_1\dot{y}_{c1}\,d\tau$. This term involves the coefficient f_n, which is related to the nonconservative inviscid force acting on the nose of the leading car. This term has a plus sign and is proportional to u; moreover, $f_n \leqslant 1$. If $\dot{\alpha}_1$ and $\dot{y}_{c1}$ have the same sign (or $\int_0^T \dot{\alpha}_1\dot{y}_{c1}\,dt>0$), then this term is always positive, and the first term on the right-hand side of Eq. (45) does work on the system.

If we let $f_n = f_t = 1.0$ in Eq. (45), only the term $(2\mu u^2/\pi)(C_T - C_N)\sum_{j=1}^N l_j\int_0^T \alpha_j\dot{y}_{cj}\,d\tau$, related to viscous forces, remains. This term consists of a summation for all the cars ($j=1$ to N) of the product of the angle α_j and the translational velocity $\dot{y}_{cj}$, that is

$$\sum_{j=1}^{N} l_j\int_0^T \alpha_j\dot{y}_{cj}\,d\tau = \sum_{j=1}^{N} l_j\overline{\alpha_j\dot{y}_{cj}} = l_1\overline{\alpha_1\dot{y}_{c1}} + l_2\overline{\alpha_2\dot{y}_{c2}} + \cdots + l_1\overline{\alpha_N\dot{y}_{cN}}.$$

Thus, each term consists of the product of variables with the *same* subscript j ($j=1,\ldots,N$) and is therefore related to the motion of one car only. If α_j and $\dot{y}_{cj}$ have the same sign (or $\int_0^T \alpha_j\dot{y}_{c1j}\,dt>0$) and $C_T - C_N > 0$ ($C_N/C_T<1$), then the term with the plus sign is always positive and does work on the system. Other terms in Eqs. (44) and (45) can be considered in the same manner.

Table 4 summarizes the conditions for all the terms in Eqs. (44) and (45) for positive work done by the fluid on the systems of the LEB and LTB models. In the columns of the table, the model considered, coefficient of term involved, sign, flow velocity, condition for positive work, and the corresponding motion of the terms are shown. In the "Motion" column, the schematic drawing of the motion for $\dot{\alpha}_1>0$ and $\dot{y}_{c1}>0$ is given. An overbar over a term means integration over a period of oscillation T (i.e. $\overline{\dot{\alpha}_1\dot{y}_{c1}} = \int_0^T \dot{\alpha}_1\dot{y}_{c1}\,d\tau$). Let us recall that "$m$" represents the number of cars for the LEB system and "j" for the LTB system in Eqs. (44) and (45), respectively. To compare the LEB and LTB models in Table 4, the notation for the LEB model has been changed to match that of the LTB model, that is, "m" has been replaced by "j."

As seen in Table 4, because most terms of the LEB model consist of summations of products of angle or angular velocities of *different* cars j and k ($j\neq k$), these terms are related to all cars from $k=1$ to N. For example, for the term in the first line of Table 4, $\sum_{j=1}^N\sum_{k=j+1}^N \overline{\dot{\theta}_k\dot{\theta}_j}<0$, the motion of cars can be explained as follows. If $N=3$, $\sum_{j=1}^3\sum_{k=j+1}^3 \overline{\dot{\theta}_k\dot{\theta}_j} = \overline{\dot{\theta}_2\dot{\theta}_1} + \overline{\dot{\theta}_3\dot{\theta}_1} + \overline{\dot{\theta}_3\dot{\theta}_2}<0$. If $\dot{\theta}_1$ has a different sign from $\dot{\theta}_2$ and $\dot{\theta}_3$ (say, $\dot{\theta}_1>0$, $\dot{\theta}_2<0$, and $\dot{\theta}_3<0$), we have $\overline{\dot{\theta}_2\dot{\theta}_1}<0$ and $\overline{\dot{\theta}_3\dot{\theta}_1}<0$. These terms satisfy the necessary condition of being negative for $\Delta W>0$. On the other hand, we also have $\overline{\dot{\theta}_3\dot{\theta}_2}>0$ at the same time; this term does not satisfy the aforementioned necessary condition of being negative. In fact, the necessary condition of a negative sign must be satisfied after the summation over all the terms $\sum_{j=1}^N\sum_{k=j+1}^N \overline{\dot{\theta}_k\dot{\theta}_j} = \overline{\dot{\theta}_2\dot{\theta}_1} + \overline{\dot{\theta}_3\dot{\theta}_1} + \overline{\dot{\theta}_3\dot{\theta}_2}<0$ has been carried out. Therefore, the motion of all the cars in the LEB model has to be considered simultaneously. As N is increased, it becomes more complicated to examine the necessary condition for obtaining a negative sign overall for the motion of the cars. In contrast, because all the terms in the LTB model consist of products of quantities associated with the *same* car j, as seen in Table 4, examination of the necessary condition for $\Delta W>0$ for the LTB model is more straightforward. This is an essential difference between the LEB and LTB systems. The full appreciation of the significance of these results will be gained in the next section.

6. Modal shapes

In the previous section, the conditio
ns for positive work in the LTB and LEB models were derived analytically and are listed in Table 4. In this section, some modal shapes of the system obtained by numerical computations will be illustrated for a period of oscillation T. They are compared with the corresponding motions in Table 4. In addition, time histories of displacement, angle, and the corresponding velocities, and their products for the cars of clamped–free and free–free LTB models at four different times in a period of oscillation ($t=0$, $T/4$, $T/2$, $3T/4$, and T) are given.

6.1. Clamped-free system

Here, the modal shapes of the clamped–free LEB model are analysed by applying the present numerical computation for the LTB model subject to the conditions $J\to 0$ and $k_\eta\to\infty$. Recall that the equations of motion of the LTB model are identical to those of the LEB one if $J\to 0$ and $k_\eta\to\infty$, as shown in Section 3.2.

Table 4
Conditions for positive work done on the systems of clamped–free LEB and free–free LTB models

Model	Term	Sign	U	Condition	Motion
LEB	m_f	$-$	U	$\sum_{j=1}^{N}\sum_{k=j+1}^{N}\overline{\dot{\theta}_k\dot{\theta}_j}<0$	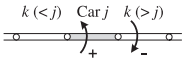
		$+$	U	$\sum_{j=1}^{N}\sum_{k=1}^{j-1}\overline{\dot{\theta}_k\dot{\theta}_j}>0$	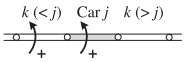
		$+$	U	$\sum_{j=1}^{N}\overline{\dot{\theta}_j^2}>0$	Always positive
	c_N	$-$	U	$\sum_{j=1}^{N}\sum_{k=j+1}^{N}\overline{\dot{\theta}_k\dot{\theta}_j}<0$	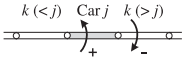
		$-$	U	$\sum_{j=1}^{N}\sum_{k=1}^{j-1}\overline{\dot{\theta}_k\dot{\theta}_j}<0$	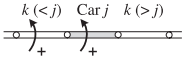
		$-$	U	$\sum_{j=1}^{N}\sum_{i=j+1}^{N}\sum_{k=1}^{i-1}\overline{\dot{\theta}_k\dot{\theta}_j}<0$	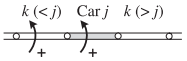
	c_T-c_N	$+^{a}$	U^2	$\sum_{j=1}^{N}\sum_{k=j+1}^{N}\overline{\dot{\theta}_k\dot{\theta}_j}>0$	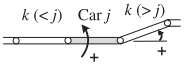
	$1-f_t$	$-$	U	$\sum_{j=1}^{N}\sum_{k=1}^{N}\overline{\dot{\theta}_k\dot{\theta}_j}<0$	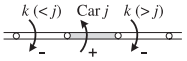
		$-$	U^2	$\sum_{j=1}^{N}\overline{\dot{\theta}_j\theta_N}<0$	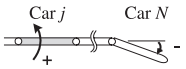
LTB	$1-f_n$	$+$	u	$\overline{\dot{\alpha}_1\dot{y}_{c1}}>0$	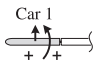
		$-$	u^2	$\overline{\alpha_1\dot{y}_{c1}}<0$	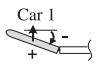
	C_T-C_N	$+^{b}$	u^2	$\sum_{j=1}^{N}\overline{\alpha_j\dot{y}_{cj}}>0$	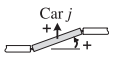
	$1-f_t$	$-$	u	$\overline{\dot{\alpha}_N\dot{y}_{cN}}<0$	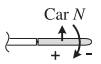
		$-$	u^2	$\overline{\alpha_N\dot{y}_{cN}}<0$	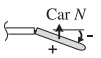

The overbar means integration over the period of oscillation T.
[a]If $c_T>c_N$.
[b]If $C_T>C_N$.

It was shown that the stability of clamped–free cylinders subjected to axial flow depends strongly on the parameter f_t (Païdoussis, 1966a, 1973). Thus, we shall focus on examining the modal shape associated with the nonconservative inviscid force involving f_t. The condition for positive work done by the fluid ($\overline{\alpha_N\dot{y}_{cN}}<0$) and the corresponding motion are shown at the bottom of Table 4. Because the nonconservative inviscid force acts only on the tapered end of the trailing car, Car N, the condition includes only the angle and the translational velocity of Car N, α_N and $\dot{y}_{cN}$. When the product of angle and translational velocity, $\alpha_N\dot{y}_{cN}$, takes a negative value over a period of oscillation, the fluid does work on the system. It is recalled that if the stiffnesses of translational springs between cars in the LTB model are sufficiently large, the LTB model may be considered as an LEB model, because the relative translational displacements

between two adjacent cars become infinitesimal. In this case, we have $\sum_{j=1}^{N} c_j\dot{\theta}_j \simeq \dot{y}_{cN}$. Then, letting $\theta_N = \alpha_N$, the condition of $\sum_{j=1}^{N}\overline{\dot{\theta}_j\theta_N} < 0$ for the LEB model can be considered to be the same as $\overline{\alpha_N\dot{y}_{cN}} < 0$ for the LTB model. The condition of $\overline{\alpha_N\dot{y}_{cN}} < 0$ can physically be explained as follows. If the tail of the trailing car keeps a downward slope ($\alpha_N < 0$) and the car moves upward ($\dot{y}_{cN} > 0$) at the same time, as illustrated at the bottom figure of Table 4, the trailing car gains energy from the fluid; here "downward" and "upward" refer to the diagrams in the table, not to the train itself.

Modal shapes of second-mode unstable oscillation of a train of six cars over a period of oscillation, $t = 0, T/4, T/2, 3T/4, T$, are illustrated in Fig. 8(b); they have been obtained numerically. The dimensional flow velocity is set at $U \simeq 4.49$ m/s, where the second mode loses stability by flutter. The overall modal constant in Fig. 8(b) may be considered to be a synthesis of first and second cantilever mode contributions. This motion can be called a "dragging motion", that is, the tangent to the free end of the model slopes backwards to the direction of motion of the free end over the greater part of a cycle of oscillation. This dragging motion is predicted to be necessary for flutter, in conjunction with the energy considerations just discussed.

Fig. 8(c) illustrates the time histories of displacement, angle, the corresponding velocities, and their products ($\alpha_N\dot{y}_{cN}$ and $\dot{\alpha}_N\dot{y}_{cN}$) for the trailing car ($N = 6$) of the clamped–free LTB model over a period of oscillation T. All the displacements and velocities tend to oscillate sinusoidally in time. However, in the bottom graph of Fig. 8(c), the product of angle and translational velocity ($\alpha_6\dot{y}_{c6}$) is seen to be almost always negative over a period of oscillation. Hence, the condition of $\overline{\alpha_6\dot{y}_{c6}} = \int_0^T \alpha_6\dot{y}_{c6}\,\mathrm{d}\tau < 0$ is clearly satisfied.

Note that the curve of the time history of $\alpha_6\dot{y}_{c6}$ has negative peaks in the quarter periods from $T/4$ to $T/2$ and from $3T/4$ to T. The absolute values of the peaks increase with increasing time because of the flutter instability, that is, the work done by the fluid increases gradually. During these periods, as seen in Fig. 8(b), the train of cars moves from one side to the other across the centreline. If we compare the modal shapes at $t = 0$ and $t = T$ in Fig. 8(b), it is seen that the translational displacement of all the cars is amplified after a period of T. On the other hand, the amplitude of $\dot{\alpha}_6\dot{y}_{c6}$ at the bottom graph of Fig. 8(c) (dotted line) is quite small (actually, $\dot{\alpha}_6\dot{y}_{c6} \simeq 0$) in comparison with that of $\alpha_6\dot{y}_{c6}$. Hence, the effect of the term $\overline{\dot{\alpha}_6\dot{y}_{c6}}$, which is proportional to U in the f_t term, may be neglected.

6.2. Free–free system with elastic supports

Recall that the dynamical behaviour of the train of free–free cars with elastic supports, whose configuration represents a simplified actual train, is given in Fig. 6(a). In this subsection, the system parameters employed are the same as those in Table 2, except for the number of cars N and the streamlining coefficient f_t. For the sake of clarity, the number of cars is set at $N = 3$, because a train of three cars is the simplest system with a middle car. Because the viscous frictional coefficients C_T and C_N have a considerable effect on the stability of the train as shown in Section 4, the streamlining coefficients are set at $f_t = 1.0$ (and $f_n = 1.0$) in order to examine the viscous frictional forces only. In this case, only the term $(2\mu u^2/\pi)(C_T - C_N)\sum_{j=1}^{N} l_j \int_0^T \alpha_j\dot{y}_{cj}\,\mathrm{d}\tau$ remains in Eq. (45). As explained in Section 4, the system becomes unstable by flutter for sufficiently high flow velocities provided that $C_T \geqslant 1.3C_N$, even though only the viscous force does positive work on the system. Consequently, we shall examine the modal shape for the effect of the viscous forces associated with C_T and C_N.

The condition for positive work done by the fluid ($\sum_{j=1}^{N}\overline{\alpha_j\dot{y}_{cj}} > 0$) and the corresponding motion are shown near the bottom of Table 4 in the row of "$C_T - C_N$." As explained in Section 5.3, the work expression does *not* include the multiplication of variables of different cars; the corresponding motion may be examined for each car. If $\dot{y}^*_{cj}$ and α_j have the same sign (or $\int_0^T \dot{y}^*_{cj}\alpha_j\,\mathrm{d}t > 0$), then the term with $C_T > C_N$ is positive and with $C_T < C_N$ negative; hence if $C_T > C_N$, the viscous forces do positive work on the system, but if $C_T < C_N$, they do negative work (hence they do not contribute to instability). That evidently explains the necessary (but not sufficient) condition for instability of $C_T > C_N$ obtained earlier.

Modal shapes of Mode 1 over a period of oscillation are illustrated in Fig. 9(a). The dimensionless flow velocity u is set at 10, where the first three modes have lost stability by flutter. If we examine the motion of each car, the condition of $\int_0^T \alpha_j\dot{y}_{cj}\,\mathrm{d}t > 0$ seems to be generally satisfied. To analyse the motion of the cars more clearly, time histories of displacement, angle, the corresponding velocities, and their products for the trailing car, Car 3, of the free–free LTB model with elastic supports over a period of oscillation T, are shown in Fig. 9(b). All the displacements and velocities tend to oscillate sinusoidally in time. On the other hand, in the bottom graph of Fig. 9(b), the product of angle and translational velocity ($\alpha_3\dot{y}_{c3}$) is almost always positive over a period of oscillation. Hence, the condition of $\overline{\alpha_3\dot{y}_{c3}} = \int_0^T \alpha_3\dot{y}_{c3}\,\mathrm{d}\tau > 0$ is clearly satisfied.

If we compare the modal shapes at $t = 0$ and T in Fig. 9(a), the translational displacement of all the cars is almost the same after a period T. On the other hand, the amplitude of $\dot{\alpha}_3\dot{y}_{c3}$ oscillates symmetrically with respect

to the zero reference line. Hence, no contribution to the work related to the $\dot{\alpha}_3\dot{y}_{c3}$ term can be expected over a period of oscillation.

In the same manner, we can examine the amplitudes of $\alpha_1\dot{y}_{c1}$ and $\alpha_2\dot{y}_{c2}$. Fig. 9(c) shows the time histories of the product of the angle and the translational velocity of Cars 1–3 over a period of oscillation T. The curve of Car 3 in Fig. 9(c) is the same as the solid line at the bottom of Fig. 9(b). The time histories show that Cars 1 and 2 oscillate like Car 3. These cars have the same period of oscillation, but there is a phase difference in their motions. All the curves clearly satisfy the condition of $\int_0^T \dot{y}_{cj}^*\alpha_j\,dt > 0$. Thus, it is confirmed that the frictional viscous term with $C_T > C_N$ has a considerable effect on the instability of the present system of a simplified model of an actual train.

7. Conclusions

The dynamical stability of a train of flexibly interconnected rigid cylindrical cars with elastic supports subjected to fluid dynamic forces simulating motion in a tunnel has been studied theoretically. The principal aim of this study was to investigate the dynamics of a high-speed train running in a tunnel, or more generally of a train-like articulated system travelling in confined fluid. The system can be treated as a lumped-parameter Timoshenko-beam (LTB) model on elastic supports, which can replicate the dynamical behaviour of an Euler–Bernoulli beam under certain conditions. The typical dynamical behaviour of the LTB model is found to be as follows: small flow velocities act to damp free oscillation of the system; as the flow velocity increases, the system becomes unstable by flutter in the lower modes.

The effect of varying the principal parameters on the dynamics of the train system of the LTB model was evaluated by calculating the critical velocities and the percentage differences with respect to a set of standard parameters. It was

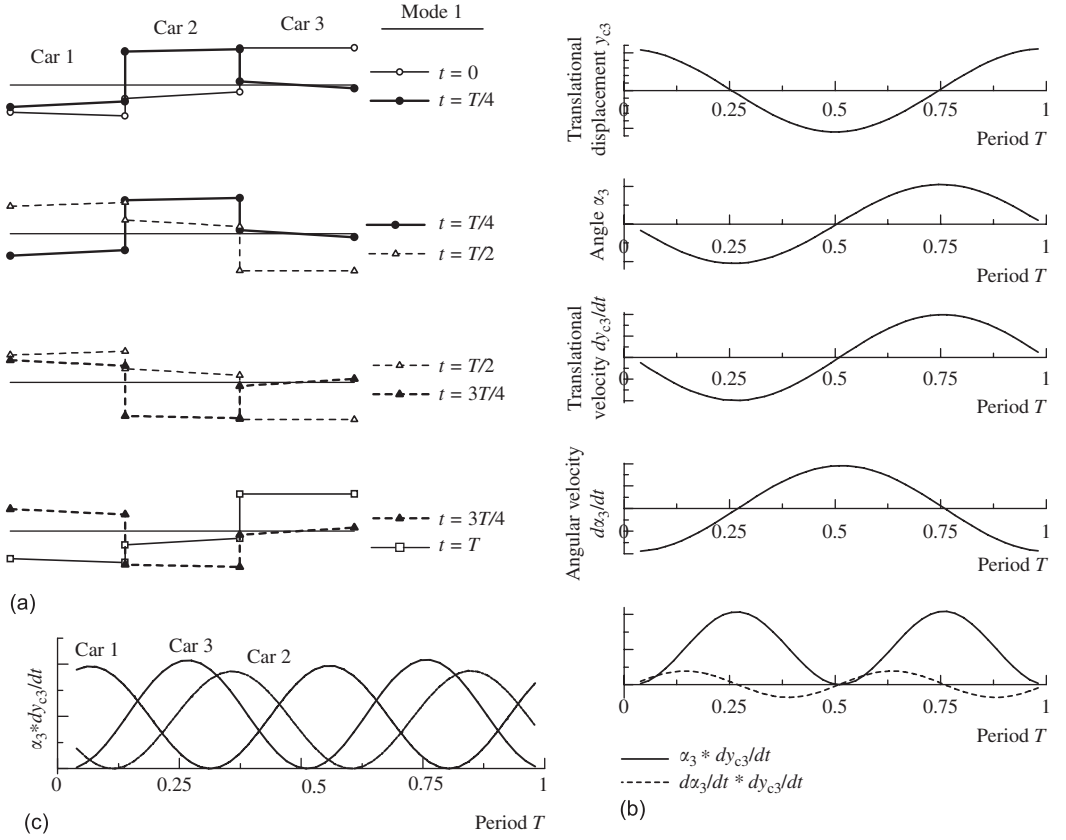

Fig. 9. (a) Modal shapes of the lowest eigenmode of LTB system over a period of oscillation, $t = 0, T/4, T/2, 3T/4, T$ ($N = 3, f_t = 1, C_N = C_T/2, u = 10$). (b) Time histories of displacement, angle, the corresponding velocities, and their products for the trailing car, Car 3, of the free–free LTB model with elastic supports over a period of oscillation T ($N = 3, f_t = 1, C_N = C_T/2, u = 10$). (c) Time histories of the product of angle and translational velocity of Cars 1–3 of the free–free LTB model with elastic supports over a period of oscillation T ($N = 3, f_t = 1, C_N = C_T/2, u = 10$).

shown that, among the aerodynamic system parameters, the ratio between viscous frictional drag coefficients in the normal and longitudinal directions, C_N/C_T, has a considerable effect on the stability of the train.

The mechanism of instability of the Lumped-parameter Timoshenko Beam (LTB) and Euler–Bernoulli Beam (LEB) models and the differences associated with these models have been studied by examining the equations of motion, the work done by the fluid, and the modal shapes for the two models. The conditions for positive work done by the fluid for the LTB and LEB models were derived analytically and discussed. An essential difference in the conditions for positive work to be done on the systems for the clamped–free LEB and free–free LTB models is the following: for the LEB model, the motion of all the cylinders (cars) has to be considered simultaneously, because the work done for the LEB model involves terms with products of different cylinder motions; conversely, for the LTB model, the work done by each cylinder can be considered separately.

In Part 2 of this study (Sakuma et al., 2008) wave propagation and flow-excited vibration of the LTB model will be studied.

References

Benjamin, T.B., 1961. Dynamics of a system of articulated pipes conveying fluid. I. Theory. Proceedings of the Royal Society of London Series A—Mathematical and Physical Sciences 261, 457–486.

Crandall, S.H., Karnopp, D.C., Kurtz, J., Edward, F., Pridmore-Brown, D.C., 1968. Dynamics of Mechanical and Electromechanical Systems. Krieger Publishing Company, Malabar, Florida.

Fujimoto, H., 1999. Research on dynamic influences of vehicle coupling and vibration in running railway vehicles. Technical Report 29 (Special), Railway Technical Research Institute (in Japanese).

Fujita, F., Shintani, A., 2001. Axial leakage flow-induced vibration of the elastic rod as the axisymmetric continuous flexible beam. ASME Journal of Pressure Vessel Technology 123, 421–428.

Fujita, F., Shintani, A., Yoshino, T., 2000. Vibrational behavior of a rigid body supported by a damper-spring system in a narrow passage fluid. In: Ziada, S., Staubli, T. (Eds.), Flow Induced Vibration. A.A. Balkema, Rotterdam, pp. 829–836.

Goodman, T.R., 1967. The aerodynamic characteristics of a slender body traveling in a tube. Oceanics Inc. Technical Report 66–31 (AIAA Journal 9, 712–717, 1971).

Goodman, T.R., Lehman, A.F., 1968. Static aerodynamic force measurements of bodies in tubes. Oceanics Inc. Technical Report 68–45.

Hamy, N., 1971. The Trebron sea chain system. Technical Report, Trebon Holdings Ltd., Montreal, Canada.

Hawthorne, W.R., 1961. The early development of the Dracone flexible barge. Proceedings of the Institution of Mechanical Engineers (London) 175, 52–83.

Inada, F., Hayama, S., 1990a. A study on leakage-flow-induced vibrations. Part I: Fluid dynamic forces and moments acting on the walls of a narrow tapered passage. Journal of Fluids and Structures 4, 395–412.

Inada, F., Hayama, S., 1990b. A study on leakage-flow-induced vibrations. Part II: Stability analysis and experiments for two degree-of-freedom systems combining translational and rotational motions. Journal of Fluids and Structures 4, 413–428.

Lighthill, M.J., 1960. Note on the swimming of slender fish. Journal of Fluid Mechanics 9, 305–317.

Manabe, K., 2002. Tetsudo niokeru hadou to shindou (Wave and Vibration Problems in Railway System). Kotsushimbunsha (in Japanese).

Mateescu, D., Païdoussis, M.P., 1985. The unsteady potential flow in an axially variable annulus and its effect on the dynamics of the oscillating rigid centerbody. ASME Journal of Fluids Engineering 107, 421–427.

Mateescu, D., Païdoussis, M.P., 1987. Unsteady viscous effects on the annular-flow-induced instabilities of a rigid cylindrical body in a narrow duct. Journal of Fluids and Structures 1, 197–215.

Miyamoto, M. (Ed.), 1994. Dynamics of Railway Vehicles. JSME (in Japanese).

Ortloff, C.R., Ives, J., 1969. On the dynamic motion of a thin flexible cylinder in a viscous system. Journal of Fluid Mechanics 38, 713–720.

Païdoussis, M.P., 1966a. Dynamics of flexible slender cylinders in axial flow. Part 1: Theory. Journal of Fluid Mechanics 26, 717–736.

Païdoussis, M.P., 1966b. Dynamics of flexible slender cylinders in axial flow. Part 2: Experiments. Journal of Fluid Mechanics 26, 737–751.

Païdoussis, M.P., 1968. Stability of towed, totally submerged flexible cylinders. Journal of Fluid Mechanics 34, 273–297.

Païdoussis, M.P., 1970. Dynamics of submerged towed cylinders. In: Eighth Symposium on Naval Hydrodynamics: Hydrodynamics in Ocean Environment. United States ONR, ARC-179, pp. 981–1016.

Païdoussis, M.P., 1973. Dynamics of cylindrical structures subjected to axial flow. Journal of Sound and Vibration 29, 365–385.

Païdoussis, M.P., 1976. Dynamics of fuel strings in axial flow. Annals of Nuclear Energy 3, 19–30.

Païdoussis, M.P., 1979. The dynamics of clusters of flexible cylinders in axial flow: Theory and experiments. Journal of Sound and Vibration 65, 391–417.

Païdoussis, M.P., 1986. Stability of a chain of cylinders travelling underwater. In: Proceedings of the Fifth International Offshore Mechanics and Arctic Engineering Symposium, Tokyo, Japan. ASME, New York, pp. 483–490.

Païdoussis, M.P., 1998. Fluid–Structure Interactions: Slender Structures and Axial Flow, vol. 1. Academic Press, London.

Païdoussis, M.P., 2003. Fluid–Structure Interactions: Slender Structures and Axial Flow, vol. 2. Elsevier Academic Press, London.
Païdoussis, M.P., Mateescu, D., Sim, W.G., 1990. Dynamics and stability of a flexible cylinder in a narrow coaxial cylindrical duct subjected to annular flow. Journal of Applied Mechanics 57, 232–240.
Porcher, G., de Langre, E., 1997. A friction-based model for fluidelastic forces induced by axial flow. In: Païdoussis, M.P., et al. (Eds.), Proceedings of the Fourth International Symposium on Fluid–Structure Interactions, Aeroelasticity, Flow-Induced Vibration and Noise, vol. II. ASME, New York, pp. 67–74.
Sakuma, Y., 2006. Dynamics of trains and train-like articulated systems travelling in confined fluid. Ph.D. Thesis. McGill University, Montreal, QC, Canada.
Sakuma, Y., Païdoussis, M.P., Price, S.J., 2008. Dynamics of trains and train-like articulated systems travelling in confined fluid. Part 2: Wave propagation and flow-excited vibration. Journal of Fluids and Structures 24, this issue, doi: 10.1016/j.jfluidstructs.2008.01.003.
Sugimoto, N., 1996. Aeroelastic stability of a beam travelling in a tunnel lined with resonators. AIAA Journal 34, 2005–2013.
Tanaka, S., Kaneko, S., Watanabe, T., 1999. Analysis of aerodynamic vibration of trains running in tunnels at high speed. In: Proceedings of the Dynamics and Design Conference 1999. p. D606 (in Japanese).
Tanaka, S., Hirata, T., Kaneko, S., Watanabe, T., 2001. Aerodynamic vibration of combined rigid bodies due to leakage flow (The effect of body shapes and support condition). In: Proceedings of ASME PVP Conference 2001, pp. 1–8.
Taylor, G.I., 1952. Analysis of the swimming of long and narrow animals. Proceedings of the Royal Society of London Series A—Mathematical and Physical Sciences 214, 158–183.
Thomson, W.T., 1993. Theory of Vibration with Applications, 4th ed. Prentice-Hall, Englewood Cliffs.
Wang, D.P., 1969. Stability of a slender elastic body traveling in a tube. Oceanics Inc. Technical Report 68-54.